

# Deep-sea stylasterid $\delta^{18}\text{O}$ and $\delta^{13}\text{C}$ maps inform sampling scheme for paleotemperature reconstructions

Theresa M. King<sup>1</sup>, Brad E. Rosenheim<sup>1</sup>, and Noel P. James<sup>2</sup>

5 <sup>1</sup>College of Marine Science, University of South Florida, St. Petersburg, 33701, USA

<sup>2</sup>Department of Geological Sciences and Geological Engineering, Queens University, Kingston, K7L 3N6, Canada

Correspondence to: Theresa M. King (theresaking@usf.edu)

**Abstract.** Deep-sea corals have the potential to provide high-resolution paleotemperature records to evaluate oceanographic changes in settings that are vulnerable to current and future ocean warming. The isotopic records preserved in coral skeletal carbonate, however, are limited by their large offsets from isotopic equilibrium with seawater. These “vital effects” are the result of biological influences (kinetic and metabolic) on the calcification of coral skeletons and are well known to drive oxygen and carbon stable isotope ratios ( $\delta^{18}\text{O}$  and  $\delta^{13}\text{C}$ , respectively) away from an isotopic signature in equilibrium with environmental variables. In this study, two stylasterid corals (*Errina fissurata*) are sampled via cross sections through their primary growth axes to create skeletal  $\delta^{18}\text{O}$  and  $\delta^{13}\text{C}$  maps. Such maps reveal a consistent trend of increasing isotopic values toward the innermost portion of the coral slices; the average center values being  $\sim 1\%$  and  $\sim 3\%$  closer to seawater  $\delta^{18}\text{O}$  and  $\delta^{13}\text{C}$  equilibrium values (respectively) than a traditional bulk sample. We investigate possible mechanisms for these unique isotopic trends, including changes in the proportions of aragonite and calcite in these mixed mineralogy corals, and potential growth patterns that would drive spatial isotopic trends. These results highlight the diversity of the stylasterid coral family and the need for additional work to establish  $\delta^{18}\text{O}$  paleotemperature calibrations for deep-sea corals of mixed mineralogy instead of purely aragonite or calcite. Despite the absence of a specific temperature calibration, we can prescribe a sampling scheme for *E. fissurata* corals to achieve accurate paleotemperature reconstructions. Additionally, vital effects of deep-sea branching corals are not well understood, thus hindering the utility of paleoceanographic archives with a vast latitudinal range. This contribution describes the likely growth structure of a deep-sea stylasterid coral taxon and demonstrates the optimal sampling location for its use in paleotemperature reconstructions. We sampled two coral specimens via cross sections through their primary growth axes to create skeletal  $\delta^{18}\text{O}$  and  $\delta^{13}\text{C}$  maps. Such maps reveal a consistent trend of increasing isotopic values toward the innermost portion of the coral slices; the average center values being  $\sim 1\%$  closer to seawater equilibrium values than a traditional bulk sample. The difference between the higher center and lower bulk  $\delta^{18}\text{O}$  values result in a temperature difference as much as  $5.1^\circ\text{C}$  ( $\pm 1.8^\circ\text{C}$ ) between the sampling methods. These results support a two-step biomineralization consisting of a rapid initial skeletal construction (stronger vital effects), followed by a slower infilling concentrated towards the center (weaker vital effects) not yet described for this coral taxon. We anticipate this work will initiate efforts to sample

~~deep sea branching corals and potentially inform advanced visualization techniques (e.g., computed tomography scans) to achieve the most accurate paleotemperature reconstructions possible.~~

## 1 Introduction

Robust paleoceanographic temperature proxies are fundamental to understanding past climate changes and sensitivities. Foundational work developed the theory and application of the oxygen isotope paleothermometer, which was applied to marine biogenic carbonates including foraminiferal tests and shallow water corals (Urey, 1947; McCrea, 1950; Epstein et al., 1953; Emiliani, 1955; Shackleton, 1967; Emiliani et al., 1978). All archives have limits in geographic distribution despite their ability to lengthen the time domain of ~~our~~ paleoceanographic records. On the Antarctic margin, for instance, foraminifera are not widely present in marine sediment cores. Scleractinian zooxanthellate corals are limited to lower latitudes. Deep-sea azooxanthellate corals have been used to elucidate ocean history on different time scales (Adkins et al., 1998; Robinson et al., 2005; Robinson and van de Flierdt, 2009; Burke and Robinson, 2012; Chen et al., 2020), but normally the extraction of continuous records from individual colonies has been precluded by the complexity of growth habit and the fidelity of elemental and isotopic records archived in their skeletons (Weber, 1973; Wisshak et al., 2009; Robinson et al., 2014). Corals can incorporate high resolution geochemical records over decades to millennia while remaining fixed to the seafloor; this is especially useful to observe regional and global processes causing ocean water masses to heave and shoal at timescales over which the coral is alive (Andrews et al., 2002; Druffel et al., 1990; Druffel, 1997; Griffin and Druffel, 1989; Risk et al., 2002). Such archives are crucial for paleotemperature reconstructions.

Biom mineralization of carbonate coral skeletons records both environmental information (~~which we treat herein as “signal”~~) and biological effects (~~noise~~, also known as “vital effects”), the latter of which must be understood to obtain high-fidelity records of ocean change. Vital effects can obscure environmental information stored in skeletal records as oxygen and carbon stable isotope ratios ( $\delta^{18}\text{O}$  and  $\delta^{13}\text{C}$ , respectively). Slow rates of calcification allow for carbon and oxygen isotopes of solid carbonate to approach isotopic equilibrium between skeleton and seawater, a state governed by thermodynamics (McConnaughey, 1989a). Biological calcification, however, includes nonequilibrium fractionation which cannot be interpreted directly as environmental signal (Weber and Woodhead, 1970). Early research on corals demonstrated that isotopic variability can be caused by metabolic fractionation, kinetic fractionation, or a combination of both (McConnaughey, 1989a). The metabolic fractionation is characterized by a change in carbon isotope composition of the dissolved inorganic carbon pool from which the coral calcifies via incorporation of the products of respiration and photosynthesis of algal symbionts or respiration of the coral itself (Swart, 1983; McConnaughey, 1989a). The kinetic fractionation is described as a product of the kinetic isotope effect: discrimination against heavy oxygen and carbon isotopes during hydration and hydroxylation of  $\text{CO}_2$  during biomineralization (McConnaughey, 1989b). Rapid calcification results in greater disequilibrium of skeletal  $\delta^{18}\text{O}$  and  $\delta^{13}\text{C}$  as the  $\text{CO}_2$  does not have sufficient time to equilibrate with ambient seawater before being incorporated into the skeleton

(McConnaughey, 1989b). ~~Additional mechanisms for vital effects have been identified more recently, including a biologically mediated pH gradient across coral cell walls (Adkins et al., 2003). Rapid biomineralization drives the pH of internal calcifying fluid toward higher values, increasing the pumping of CO<sub>2</sub>, and consequently maximizing fractionation of carbon isotopes (Adkins et al., 2003). Chen et al. (2018) then combined these findings with an additional constraint of kinetic fractionation by the carbonic anhydrase enzyme which catalyzes the hydration and hydroxylation of CO<sub>2</sub> and constructed the most comprehensive model for biomineralization to date.~~

~~Vital effects have been invoked to explain skeletal  $\delta^{18}\text{O}$  and  $\delta^{13}\text{C}$  values lower than equilibrium, and the~~ ~~Because coral specimens from varied ocean depths and latitudes have a strong linear relationship between skeletal  $\delta^{18}\text{O}$  and  $\delta^{13}\text{C}$  values~~ ~~has been used to further understand vital effects exhibited by corals from varied ocean depths and latitudes (Smith et al., 2000; Emiliani et al., 1978; Heikoop et al., 2000; Mikkelsen et al., 2008; McConnaughey, 1989a), vital effects have been employed to discern trends in  $\delta^{18}\text{O}$  and  $\delta^{13}\text{C}$  records from deep sea corals. Early work by Emiliani et al. (1978) examined the  $\delta^{18}\text{O}$  and  $\delta^{13}\text{C}$  recorded by a solitary scleractinian coral (class Hexacorallia, order Scleractinia) and found that both isotopic ratios trended toward higher values from the bottom to top of the coral. This was interpreted as a slowing growth rate with time, approaching isotopic equilibrium with the surrounding seawater (Emiliani et al., 1978). Additional work on solitary scleractinians by Adkins et al. (2003) employed a microsampling approach for  $\delta^{18}\text{O}$  and  $\delta^{13}\text{C}$  that identified new mechanisms for vital effects. Along with the lowest isotopic values occurring at regions of rapid calcification, Adkins et al. (2003) observed a break in the linear relationship of stable isotopic ratios in these regions. The authors hypothesized that rapid biomineralization drives the internal calcifying fluid pH toward higher values, increasing the pumping of CO<sub>2</sub> inward, which stabilizes fractionation of carbon isotopes, yet further fractionates oxygen isotopes due to pH driven changes in carbonate speciation (Adkins et al., 2003). Later work on bamboo corals (class Octocorallia, order Malacalcyonacea) sampled across and along their vertical growth axes resulted in low  $\delta^{18}\text{O}$  and  $\delta^{13}\text{C}$  values near the innermost portion of the coral and at the distal tips (Hill et al., 2011). Interpreting the lower isotope ratios, however, was complicated because the assumed faster calcification rates in these regions were not supported by calculated growth rates, and the locations of maximum growth rates were not consistent for a single specimen (Hill et al., 2011). A further understanding of vital effects was established by Chen et al. (2018) who investigated the role of the carbonic anhydrase enzyme which catalyzes the hydration and hydroxylation of CO<sub>2</sub>. The authors determined that the amount of the enzyme in the calcifying fluid determines the internal speciation of carbonate and thus, alters the slope of the linear  $\delta^{18}\text{O}$  and  $\delta^{13}\text{C}$  relationship (Chen et al., 2018).~~

~~Isotopic records have largely demonstrated sensitivity to variable rates of calcification. Early work by (Emiliani et al., 1978) examined the  $\delta^{18}\text{O}$  and  $\delta^{13}\text{C}$  recorded by a solitary scleractinian coral and found that both isotopic ratios trended toward higher values from bottom to top of the coral and interpreted this as a slowing growth rate with time, approaching isotopic equilibrium. Additional work on solitary scleractinians by Adkins et al. (2003) employed a microsampling approach for  $\delta^{18}\text{O}$  and  $\delta^{13}\text{C}$  that determined the lowest isotopic values occurred at trabecular centers which exhibited the most rapid rates of calcification and~~

were farthest from equilibrium. Bamboo corals sampled across and along their vertical growth axes exhibited low  $\delta^{18}\text{O}$  and  $\delta^{13}\text{C}$  values near the innermost portion of the coral and at the distal tips (Hill et al., 2011). Faster calcification in these regions, however, were not supported by calculated growth rates, and there was no consistency among regions of maximum growth rates for a single specimen (Hill et al., 2011). The need for accurate paleotemperature archives underscores the need to understand the impact of vital effects on deep-sea corals. Stylasterid corals (class Hydrozoa, order Anthoathecata) are a ubiquitous taxon of deep-sea corals that occupy ocean depths from the surface to greater than 2700 m, and can be found in high and low latitudes, having great potential for paleoceanographic reconstructions (Cairns, 2011). Stylasterid geochemical work has expanded over the last several years, but because of the inherent diversity of this coral family, research is still needed to understand vital effect-induced isotope fractionation. Early work by Weber and Woodhead (1972) demonstrated that shallow water stylasterids (genus *Distichopora* and *Stylaster*) had precipitated their skeletons closer to isotopic equilibrium than some scleractinian corals. Later work by both A study by Wisshak et al. (2009) and Black and Andrus (2012) and another by Samperiz et al. (2020) examined possible diagenetic effects on the stable isotopic geochemistry of sampled stylasterid corals *Errina dabneyi* and *Stylaster erubescens*, respectively, in transects similar to Hill et al. (2011) and resulted in  $\delta^{18}\text{O}$  and  $\delta^{13}\text{C}$  trends. More recently, Samperiz et al. (2020) have produced a compilation of stylasterid skeletal  $\delta^{18}\text{O}$  and  $\delta^{13}\text{C}$  records from nearly 100 specimens. Similar to the deep-sea scleractinian corals, Samperiz et al. (2020) found the lowest  $\delta^{18}\text{O}$  and  $\delta^{13}\text{C}$  with lowest values in the innermost portion of the main coral trunk and at the distal growth tips, supporting rapid growth in those regions. This work also found that skeletal mineralogy influences  $\delta^{18}\text{O}$  and  $\delta^{13}\text{C}$  values, whereby calcitic stylasterids record slightly lower values than their aragonitic counterparts (Samperiz et al., 2020). Stylasterid carbonate skeletons can consist of aragonite, calcite, or a mixture of both polymorphs (Cairns and Macintyre, 1992; Kershaw et al., 2023). Another characteristic thus far unique to stylasterids is the absence of pH upregulation within the calcifying fluid (Stewart et al., 2022). The analysis of boron isotopes from calcitic, aragonitic, and mixed stylasterids (*Errina* spp and *Stylaster* spp) compared to those of scleractinian corals support a completely different calcification method wherein stylasterids do not elevate internal pH to promote calcification (Stewart et al., 2022). A largely unknown calcification strategy, paired with variable mineralogy that could impact stable isotopic records highlight a need to develop a deeper understanding of these corals so that we may accurately reconstruct paleoceanographic conditions. However, Samperiz et al. (2020) noted variability among the  $\delta^{18}\text{O}$  and  $\delta^{13}\text{C}$  values within a single growth band (which should represent contemporaneous calcification) as well as variability in isotopic fractionation among different genera and species of stylasterid, supporting heterogeneous calcification. Cumulatively, these results obscure best practices for colony scale sampling of deep sea corals for isolating vital effects to develop robust temperature reconstructions.

Here we focus on the small scale isotopic changes in a stylasterid taxon with the aim of understanding the best sampling approach for accurate paleotemperature reconstructions using a single species. Stylasterids are ubiquitous in both latitudinal and depth range, yet remain underrepresented in paleoceanographic reconstructions, due in part to the lack of understanding of calcification processes (Cairns, 1992). Studies have recently begun to demonstrate the utility of deep sea stylasterid taxa as

reliable archives of ocean temperature via  $\delta^{18}\text{O}$  and trace metals (Samperiz et al., 2020 and Stewart et al., 2020, respectively) as well as productivity/seawater nutrient content via skeletal Ba/Ca (Kershaw et al., 2023). To apply such archives to high-resolution reconstructions, however, a thorough understanding of the small-scale variability in vital effects is paramount. Here we establish a link between isotopic changes and deep-sea coral growth pattern of a deep-sea stylasterid and isotopic changes, using two deep-dwelling (400 to 600 m) stylasterid coral specimens, *Errina fissurata*, specimens. We generate to create  $\delta^{18}\text{O}$  and  $\delta^{13}\text{C}$  maps over coral surfaces perpendicular to and along vertical growth axes to evaluate the locations and magnitudes of isotopic variability. We complement recent work by Samperiz et al. (2020) that has demonstrated the utility of stylasterids to accurately record changes in ocean temperatures by isolating kinetic effects in deep, azooxanthellate stylasterids. We compare our skeletal maps to calculated seawater equilibrium values, mineralogical data, and isotopic trends modelled from hypothesized coral growth scenarios to determine the influences on  $\delta^{18}\text{O}$  and  $\delta^{13}\text{C}$  and potential implications for paleoceanographic reconstructions, and determine that although contradictory to previous research, the isotopic values most representative of environmental signals in these corals are recorded in the innermost portion of the coral stems. Ultimately, we prescribe targeted sampling, avoiding the use of bulk drilling methods for the most accurate paleotemperature reconstructions for *E. fissurata*.

## 2 Methods

### 2.1 Study location and specimen collection

The Ross Sea is a region of bottom water formation for the world's oceans, a characteristic that influences the local oceanography in which the stylasterids live. The region experiences seasonal katabatic winds that create sea ice-forming polynyas, which in turn, create High Salinity Shelf Water through the process of brine rejection (Kurtz and Bromwich, 1985; Picco et al., 2000). The High Salinity Shelf Water flows along the western Ross Sea and out to the shelf edge where it mixes with upwelled modified Circumpolar Deep Water, resulting in a component of dense Antarctic Bottom Water that spills down the continental slope (Gordon et al., 2009; Jacobs et al., 1970; Sandrini et al., 2007).

The stylasterid coral specimens for this study were collected aboard the U.S. Antarctic Program expedition

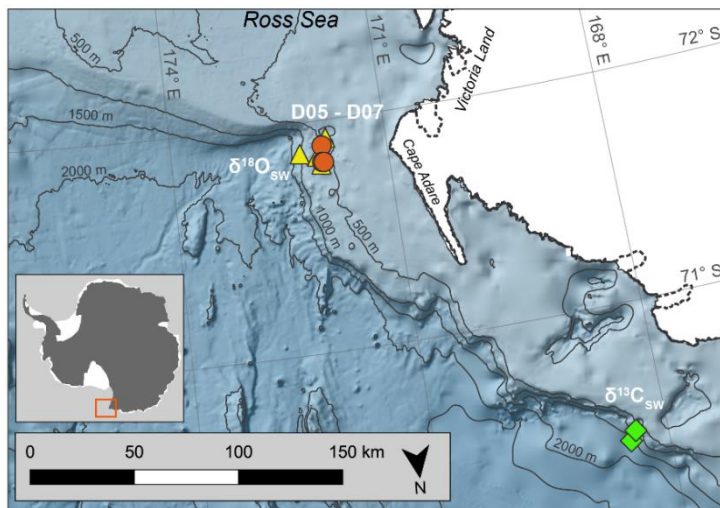


**Figure 1:** Map of coral collection sites. D05–D07 represent dredge sites during NBP07-01 from which coral samples were collected on the outer western Ross Sea continental shelf. The diamonds and triangles mark the stations used to calculate the seawater isotopic ratios ( $\delta^{13}\text{C}_{\text{sw}}$  and  $\delta^{18}\text{O}_{\text{sw}}$ ; Table S2 in the Supplement). Antarctic landmass and ice sheets are colored white (Gerrish et al., 2022) with the coastline marked by a solid black line, and ice sheet grounding line denoted by a dotted black line (Mouginot et al., 2017). Bathymetric contours are in increments of 500 m (Arndt et al., 2013). Antarctic inset denotes sampling site marked by red box. Map was created using the Quantarctica data set collection within QGIS (Matsuoka et al., 2021).

NBP07-01 near Cape Adare in the western Ross Sea. Seamounts on the outer continental shelf were dredged at a water depth ranging 400 m to 600 m and the corals used here were from the fifth through seventh dredges (D05–D07; Fig. 1, Table 1). The

recovered stylasterid corals	Lat. (°S)	Long. (°E)	Water Depth (m)	Dredge	Temp. at Depth (°C)	$\delta^{18}\text{O}$ seawater (‰, SMOW)	$\delta^{13}\text{C}$ seawater (‰, PDB)
were predominantly <i>Errina</i>	71.89	171.9	490-593	D05	$-0.10 \pm 0.09$	$-0.26 \pm 0.06$	$0.66 \pm 0.05$
spp., most likely <i>Errina</i>	71.82	171.92	518-643	D06			
<i>fissurata</i> based on	71.82	171.9	489-599	D07			

morphological descriptions (Cairns, 1983a, b, 1991) and scanning electron microscopy (SEM). Specimens were recovered both alive and dead (as evidenced by their pigmentation), some with growth tips intact. For this study, one live-collected and one dead-collected stylasterid were selected for isotopic analyses (EA-11 and EA-12, respectively), targeting the longest whole specimens ranging from ~9 to 10 cm long (Fig. 2). For SEM analyses, different corals from the same dredge were analyzed as they were sputter-coated in gold palladium and not suitable for geochemical analysis. Specimens EA-20 and EA-21 were used for taxonomical identification and EA-22 through EA-24 for physical evidence of diagenesis (e.g., Wisshak et al., 2009).

## 2.2 Coral sampling and isotope analysis

The stylasterid specimens were sampled for stable oxygen and carbon isotope measurements ( $\delta^{18}\text{O}$  and  $\delta^{13}\text{C}$ , respectively) over cross sections of their major growth axes. A Gryphon diamond band saw was used to slice discs measuring approximately 2–3 mm thick from each specimen's main stems (three from EA-11 and two from EA-12; Fig. 2). Additionally, a longer 8 mm thick section was cut from the lower main stem of EA-11 (EA-11d; Fig. 2). This disc was sliced in half lengthwise with the band saw and sampled along the vertical face. Each coral disc was sonicated in DI water until no remaining loose particles were released then dried in a 50° C oven for 24 hours. The coral discs were then drilled over their surfaces with a New Wave MicroMill system at grid spacing that varied between 1 and 1.5 mm, based on the diameter of the slice and ampullae in the disc. The MicroMill was configured with a 0.5 mm round carbide bur bit for



**Figure 2:** Whole coral specimens EA-11 (left) and EA-12 (right). EA-11 was live-collected, and EA-12 was dead. Sample discs are labelled, and the corresponding isotope maps are in Fig. 3.

each hole that plunged to a maximum depth of 1 mm, just far enough to obtain enough carbonate material for analysis (~80–120  $\mu\text{g}$   $\text{CaCO}_3$ ). The carbonate powder from each hole was transferred to vials and the sample hole and stylasterid surface were cleaned with compressed air or nitrogen to remove any residual powder between drilling intervals.

Coral Slice	$\delta^{18}\text{O}$ (‰, PDB)		$\delta^{13}\text{C}$ (‰, PDB)		n
	Maximum	Minimum	Maximum	Minimum	
EA-11a	2.48	0.65	-3.72	-9.56	17
EA-11b	2.18	0.87	-4.34	-8.61	24
EA-11c	2.64	1.08	-2.84	-8.54	20
EA-11d	2.87	0.66	-2.64	-8.68	37
EA-12a	2.81	0.60	-3.19	-8.18	17
EA-12b	2.53	0.82	-3.00	-8.02	25
All	2.87	0.60	-2.64	-9.56	140
Linear Regression (All data)	Slope	Intercept	$R^2$	p-value	n
	2.88 ( $\pm 0.14$ )	-10.94 ( $\pm 0.22$ )	0.76	< 0.001	140

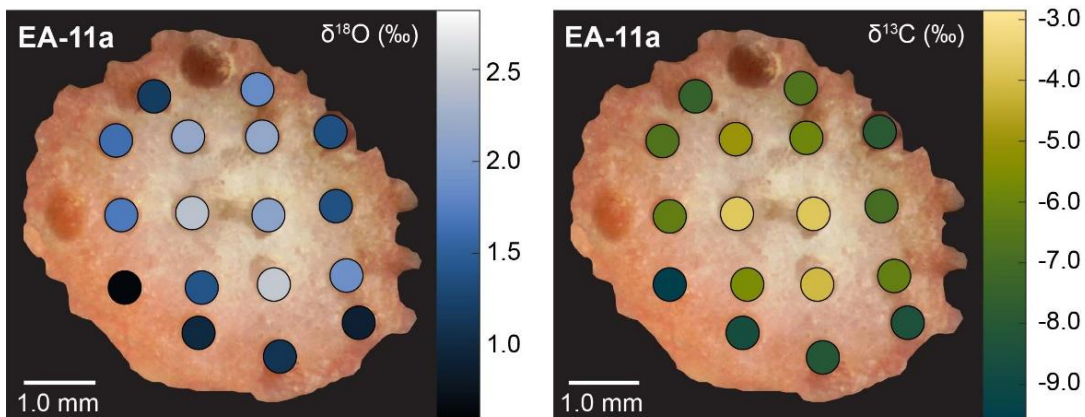
**Table 2:** Summary data for *E. fissurata* and regression statistics for the resulting compilation (see Fig. 4).

The sample vials were flushed with helium and acidified with phosphoric acid at 50° C to generate  $\text{CO}_2$  that was analyzed at the University of South Florida College of Marine Science using a Thermo Scientific MAT 253 stable isotope ratio mass spectrometer with a Gas Bench II preparatory device. All reported values are in standard delta ( $\delta$ ) notation and reported as per mil (‰). Laboratory reference materials Borba ( $\delta^{13}\text{C}$ : 2.89 ‰,  $\delta^{18}\text{O}$ : -6.15 ‰), TSF-1 ( $\delta^{13}\text{C}$ : 1.95 ‰,  $\delta^{18}\text{O}$ : -2.20 ‰), and Leco ( $\delta^{13}\text{C}$ : -15.44 ‰,  $\delta^{18}\text{O}$ : -20.68 ‰), were used for instrument correction and normalizing to the Pee Dee Belemnite scale (PDB), and an internal Antarctic coral standard was used for quality control. [To account for fractionation of oxygen isotopes during acidification \(Kim et al., 2007\) we measured calcite reference materials, which corrected for fractionation during the transfer onto the PDB scale.](#) The analytical uncertainty ( $1\sigma$ ) of the MAT 253 during this study was  $\pm 0.083$  ‰  $\delta^{13}\text{C}$  and  $\pm 0.064$  ‰  $\delta^{18}\text{O}$ .

### 2.3 Mineralogical analysis

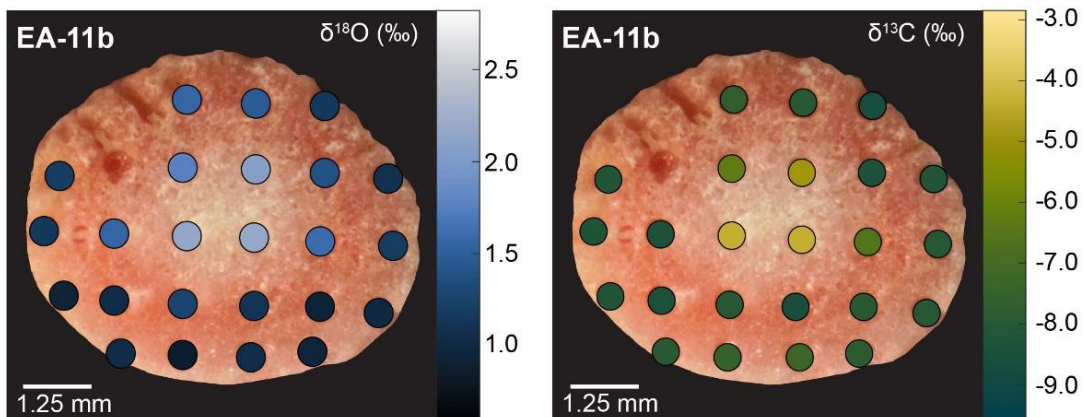
[Coral slice EA-11d was analyzed for mineralogical analysis using X-ray diffraction \(XRD\) after it was sampled for stable isotope analysis. The flat surface was not powdered, but rather scanned to isolate each vertical stripe across the pink, white, and pink colors \(Fig. 3\). The diffraction data were collected on a Bruker D8 Advance Powder Diffractometer with Lynxeye detector and motorized slits assembly at the University of South Florida X-ray Diffraction Facility and Solid State Characterization Core Lab. The coral slice was centered within a beam of very small divergence, 0.02°, that was able to probe a single band of color at a time. The crystalline phases were identified with Bruker-EVA 7 software and the Crystallographic Open Database \(COD\). Two separate additional \*E. fissurata\* specimens were sampled for mineralogical analysis via X-ray diffraction \(XRD\), one live-collected and one dead-collected \(EA-13 and EA-14, respectively\). Two samples were collected from each specimen, one in the center, white region and the other in the mid to outer pink region. The samples were ground, mixed with a quartz standard, and smeared on a glass slide. They were analyzed on a Malvern Panalytical Empyrean Multipurpose Diffractometer at Queen’s University Facility for Isotope Research, Ontario, Canada. Original total mineralogy](#)

was ascertained by running from 20.0–45.0 20. Detailed mineralogy was determined by running from 34.0–35.5 20. The reported relative mineralogical amounts are semi-quantitative.

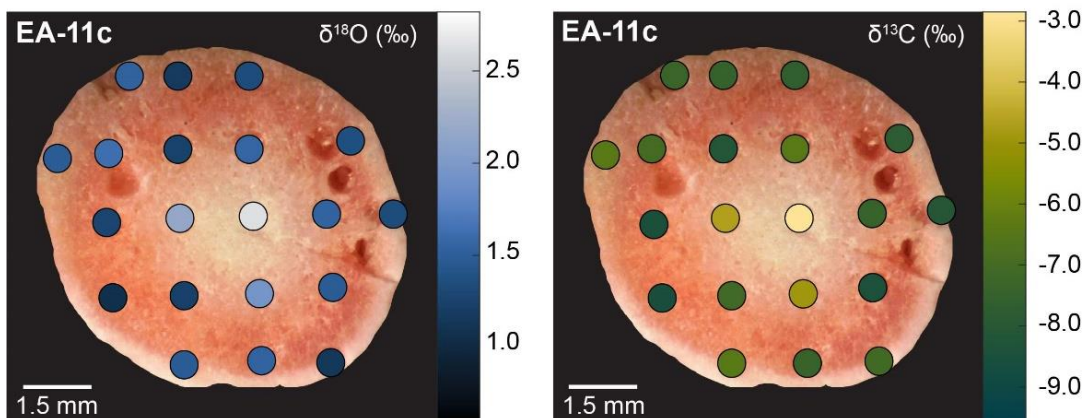


**3 Results**

The interior coral skeletons lacked any visible banded growth structure that we expected to see in the manner of Samperiz et al. (2020) and



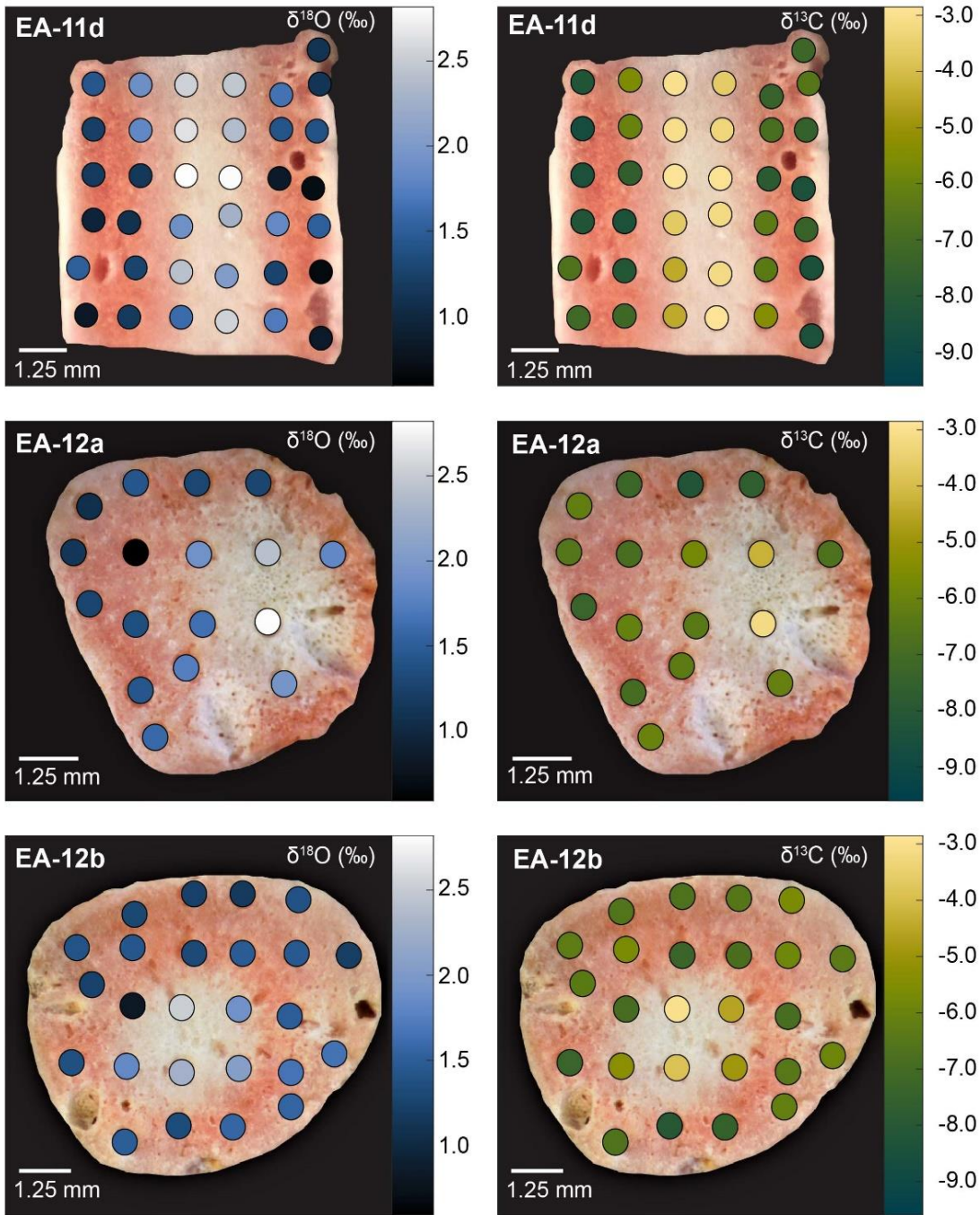
Wisshak et al. (2009). Instead, the corals were characterized by a central white section, surrounded by shades of pink in the mid to outer sections (Figs. 2 and 3). The replacement of a high-density growth



banding structure with the observed color blocking is an obstacle to estimating the amount of time over

**Figure 3:** Stable isotope ratio maps for slices from specimens EA-11 and EA-12. Each horizontal pair of images show data from the same coral slice: the left column depicts  $\delta^{18}\text{O}$  values and the right column  $\delta^{13}\text{C}$  values. The measurements are presented as colored circles on each slice with corresponding adjacent color bar. Values are expressed in per mil (‰) relative to PDB, and analytical uncertainty ( $1\sigma$ ) during this study was  $\pm 0.064$  ‰  $\delta^{18}\text{O}$  and  $\pm 0.083$  ‰  $\delta^{13}\text{C}$ . All slices exhibit the same feature of the highest isotopic values toward the inner white section, which is not always the geometric center of the slice.





which these corals have been growing. Thus, researchers aiming to [analyze/employ](#) this coral taxon must employ additional radiometric dating techniques (e.g., Cheng et al., 2000) that are beyond the scope of this work. Although there were no visible banding targets for sampling stable isotopes, the grid spacing of our sampling scheme allowed for microdrilling of several representative samples of both pink and white areas across each coral slice (Fig. S1 in the Supplement).

Figure 3 continued.

### 3.1 Stable carbon and oxygen isotope trends

285 Each coral slice exhibits a wide range of  
stable carbon and oxygen isotope ratios that  
are higher in the center, white section, and  
lower in the outer pink section of the coral  
(Fig. 3; [Table S1 in the Supplement](#)). For  
290 specimen EA-11, the ranges in  $\delta^{18}\text{O}$  and  $\delta^{13}\text{C}$   
values across slices EA-11a through EA-11c  
are  $\sim 1.5\text{‰}$  and  $\sim 5.2\text{‰}$ , respectively. This  
variability is too large to produce accurate  
paleoceanographic records without  
295 knowledge of where the most accurate, or  
closest to that of an environmental signal, is  
preserved in the coral skeleton. The slightly  
larger range of  $\delta^{18}\text{O}$  and  $\delta^{13}\text{C}$  values  
observed over EA-11d ( $2.2\text{‰}$  and  $6.0\text{‰}$ ,

300 respectively) is not as surprising as it could  
be due to the sampling scheme for this slice  
covering a larger vertical distance of coral  
than the others (i.e., transecting more time  
intervals). The compilation of EA-11  $\delta^{18}\text{O}$   
305 values ranges from  $0.65\text{‰}$  to  $2.87\text{‰}$ , and  
the  $\delta^{13}\text{C}$  values range from  $-9.56\text{‰}$  to  $-2.64\text{‰}$ ,  
with the minimum values exhibited by  
EA-11a (nearest the tip) and maximum

310 “bulk” values that would be obtained by more traditional coral drilling methods, which average isotopic compositions by  
drilling into the side of a coral, there is no significant change in either isotopic composition up-coral (Fig. 4).

For specimen EA-12, the range of  $\delta^{18}\text{O}$  and  $\delta^{13}\text{C}$  values over each of the slices is on the order of  $\sim 2\text{‰}$  and  $\sim 5\text{‰}$ , similar to  
EA-11 (Table 2). The entire range of measured EA-12  $\delta^{18}\text{O}$  values is  $0.60\text{‰}$  to  $2.81\text{‰}$ , and  $\delta^{13}\text{C}$  values range from  $-8.18\text{‰}$   
315 values, however, were not on the same slice (maximum  $\delta^{18}\text{O}$  at EA-12a and maximum  $\delta^{13}\text{C}$  at EA-12b). Similar to EA-11,  
EA-12 also exhibits variability within each slice; however, this also leads to the bulk calculations not being significantly

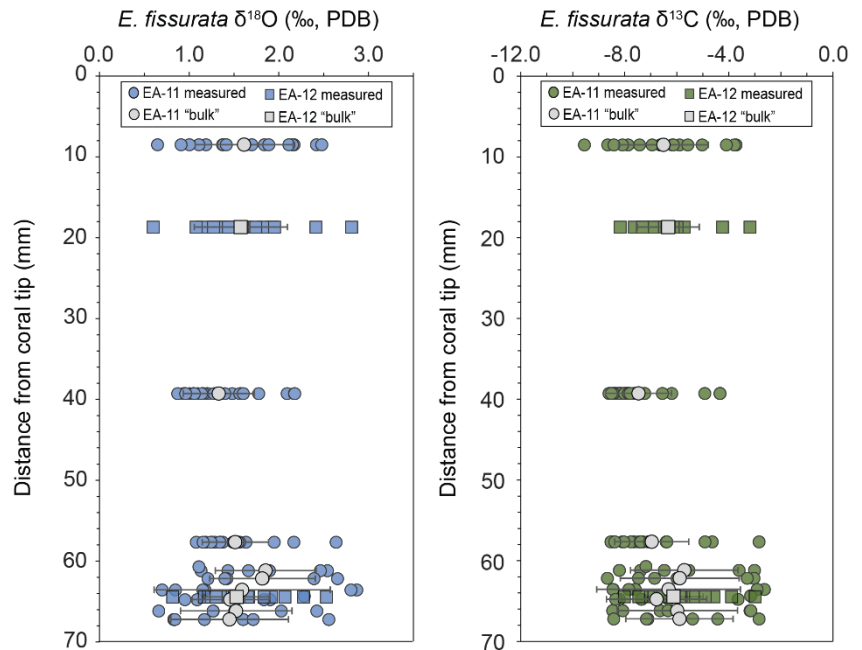


**Figure 4:** Stable isotope ratios from each slice ( $\delta^{18}\text{O}$  on left and  $\delta^{13}\text{C}$  on right) versus distance from the coral tips. On the left is  $\delta^{18}\text{O}$  and on the right is  $\delta^{13}\text{C}$ ; the analytical uncertainty for each is smaller than the data points. A “bulk” value was calculated as the average for each slice that would be similar to common bulk drilling methods (except for EA-11d which was cut transverse to the growth axis and has spans a range of distances, each averaged separately, different distances) that would be similar to a bulk drilling method. Error bars on “bulk” calculations represent standard deviation for each slice (or distance from the tip). The “bulk” values from each slice and/or distance do not vary along the growth axis, especially relative to the variability observed in each slice (see Fig. 3).

different from each other up-coral (Fig. 4). Looking closer at the individual slices from each coral, the variable stable isotope compositions are significant, i.e., the minimum and maximum values measured on each slice are well beyond the analytical uncertainty (Figs. 4 and 5). This supports that all measurements consistently demonstrate significantly higher  $\delta^{18}\text{O}$  and  $\delta^{13}\text{C}$  values in the center of each slice (Figs. 3 and 5).

### 3.2 Deviations from equilibrium with seawater $\delta^{18}\text{O}$ and $\delta^{13}\text{C}$

To determine where the *E. fissurata* corals skeletons record isotopic compositions closest to an environmental signal, we calculated carbonate isotopic equilibrium values using data reported for nearby hydrographic stations. The seawater stable isotope ratios and temperature were determined using the average composition of the 490–650 m depth range (similar to the coral collection depths; Table S2 in the Supplement) at stations nearest the coral dredge sites (Fig. 1). For seawater  $\delta^{18}\text{O}$ , we gathered seawater temperature, potential temperature, and salinity records from CTD cast data from the AnSlope (Cross-slope exchanges at the Antarctic Slope Front) project that sampled very close to our dredge sites (Fig. 1 and Fig. S2 in the Supplement) (Jacobs, 2015; Visbeck, 2015; Gordon, 2016). The average potential temperature ( $-0.12 \pm 0.09^\circ\text{C}$ ) and salinity ( $34.7 \pm 0.002$ ) were used to identify the water mass at

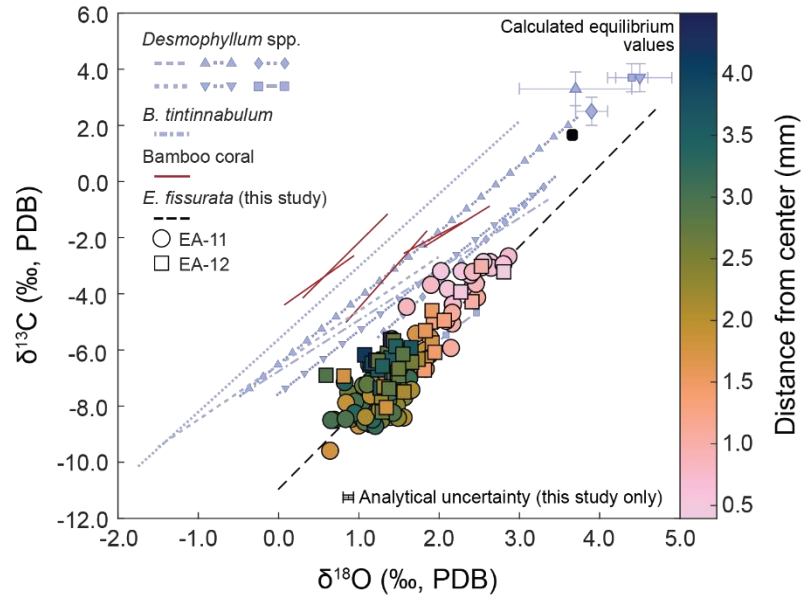


**Figure 5:** Linear regressions of  $\delta^{18}\text{O}$  vs  $\delta^{13}\text{C}$  values for *E. fissurata* compared to aragonitic scleractinian and calcitic bamboo corals. (colored circles, and black dashed line) compared to scleractinian and bamboo corals (purple and red lines, respectively). Lines for external data are not extrapolated beyond the range of reported  $\delta^{18}\text{O}$  values. Colors of circles (EA-11) and squares (EA-12) corresponds to distance from the coral center, see color bar at the right. Calculated seawater equilibrium values for *E. fissurata* is also shown as a black rounded square (uncertainty is smaller than the square). (relative to calcite) and circle (relative to aragonite). The dashed black line represents the line of best fit for the measured values isotopic values measured here ( $\delta^{13}\text{C} = 2.88 (\pm 0.14) * \delta^{18}\text{O} - 10.94 (\pm 0.22)$ ). Linear regressions for *D. cristagalli* and *Lophelia-Desmophyllum* spp. are reported by Adkins et al. (2003) and include *Desmophyllum* sp. (purple line with squares) and *D. dianthus* (all other *Desmophyllum* lines). and the dashed lines with shapes have corresponding equilibria displayed (matching shape with error bars in upper right corner). Each *D. cristagalli* specimen is labelled by its locale and the *Lophelia* specimen was recovered from the NE Atlantic. The *Bathysammia tintinnabulum* was recovered from the Blake Plateau and data are reported by Emiliani et al. (1978); and Bamboo coral data are from Hill et al. (2011), collected from the California margin. Lines for external data are not extrapolated beyond the range of reported  $\delta^{18}\text{O}$  values. The slope of the linear regression produced in this study is similar to those reported for other deep-sea corals, with a similar decrease in both isotopic ratios from equilibrium. Additionally, the measured values here that are closest to equilibrium are those toward the center of each coral disc, as noted by the lighter colors.

our locale and depth as Low Salinity Bottom Water, as described by Jacobs et al. (1985; Table S2 in the Supplement). The reported  $\delta^{18}\text{O}$  for this water mass is  $-0.26 \pm 0.06$  ‰ (Jacobs et al., 1985).

The results from XRD analyses support the dominant presence of calcite with small amounts of aragonite in these specimens. The color stripes that were analyzed from EA-11d show only small differences between the white and pink compositions (Fig S3 in the Supplement). The powdered samples of EA-13 and EA-14 yielded similar results of mixed mineralogy with ~70 to 77 % calcite (~30 to 23 % aragonite) in the center white portions and ~75 to 80 % calcite (~25 to 20 % aragonite) in the outer pink regions (Table 3). Although there is evidence for mixed mineralogy here, we calculate seawater equilibrium values relative to calcite as that is the main component. With the seawater  $\delta^{18}\text{O}$  and average seawater temperature within our depth range, we calculated the equilibrium carbonate  $\delta^{18}\text{O}$  value was calculated to be as  $3.66 \pm 0.06$  ‰ for calcite and  $4.51 \pm 0.06$  ‰ for aragonite using the equations from O'Neil et al. (1969), and Grossman and Ku (1986), respectively. Determining seawater  $\delta^{13}\text{C}$  was straightforward as direct measurements existed for nearby WOCE (World Ocean Circulation Experiment) stations (Fig. 1 and Fig. S2 in the Supplement) (WOCE, 2002). Using the average of reported seawater  $\delta^{13}\text{C}$  values for our depth range ( $0.66 \pm 0.05$  ‰), we

calculated the equilibrium carbonate  $\delta^{13}\text{C}$  values as  $1.66 \pm 0.20$  ‰ for calcite and  $3.36 \pm 0.60$  ‰ for aragonite with the equations from Romanek et al. (1992) (Fig. 5; Table S2 in the Supplement). We calculated equilibrium values for both calcite and aragonite because stylasterids have exhibited mixed mineralogy, and we have evidence for that here (Cairns and Macintyre, 1992; Sect. 4.2.3).

Each coral slice exhibits a significant offset from the calculated equilibrium values, with the smallest

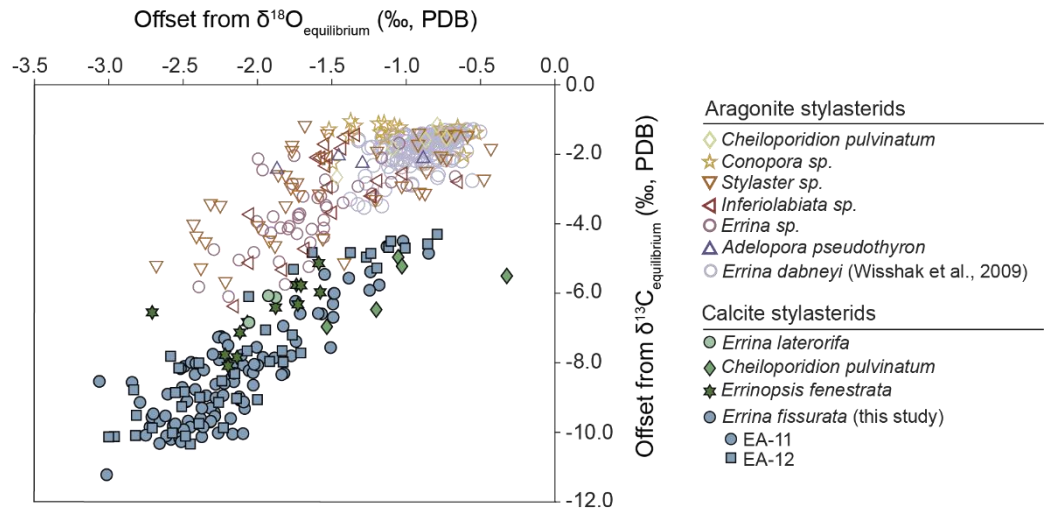


**Figure 6:** Difference between measured coral isotope ratios and equilibrium values for compilation of stylasterid corals. Except for *E. dabneyi* and *E. fissurata*, all coral isotope data are from Samperiz et al. (2020) and the corresponding equilibrium values were calculated using corresponding seawater data from Samperiz et al. and equations from Grossman and Ku (1986; aragonite  $\delta^{18}\text{O}$  equilibrium), O'Neil et al. (1969; calcite  $\delta^{18}\text{O}$  equilibrium), and Romanek et al. (1992; aragonite and calcite  $\delta^{13}\text{C}$  equilibrium). *Errina dabneyi* data and  $\delta^{18}\text{O}$  equilibrium are from Wisshak et al. (2009), and the  $\delta^{13}\text{C}$  equilibrium was calculated using reported seawater data from Wisshak et al. (2010). Filled symbols represent all *Errina* specimens. The corals from this study (blue filled circles and squares) exhibit a similar offset from equilibrium to other calcitic specimens (filled symbols). Some of the values closer to equilibrium (relative to calcite) from the *E. fissurata*, even overlap with aragonitic samples as well. Note that stylasterid data shown in Figure 6 are included here.

offsets located in the center of each coral slice (Figs. 5, 6, and 7). These equilibrium offsets are all negative in direction (i.e., the corals record isotopic ratios less than expected equilibrium) and range from -3.0694 to -0.79 ‰ for  $\delta^{18}\text{O}$  and from -11.222-92 to -4.30 ‰ for  $\delta^{13}\text{C}$  (Fig. 6). The offsets from  $\delta^{13}\text{C}$  equilibrium are considerably ~~stently~~ larger than those of  $\delta^{18}\text{O}$ , and the offsets relative to aragonite equilibrium are larger than those calculated relative to calcite equilibrium (Fig. 6). Additionally, we observe a strong linear correlation between  $\delta^{18}\text{O}$  and  $\delta^{13}\text{C}$  values. The compilation of samples in this study result in a linear trend with a slope of  $2.88 \pm 0.14$  ( $\Delta\delta^{13}\text{C}/\Delta\delta^{18}\text{O}$ ;  $R^2=0.76$ ) or  $0.26 \pm 0.01$  ( $\Delta\delta^{18}\text{O}/\Delta\delta^{13}\text{C}$ ;  $R^2=0.76$ ) that passes near the calculated equilibrium values (Fig. 5 and Table 2). Most noticeable is that the values measured from closest to the center of the coral slice are consistently closest to calculated equilibrium, whereas the values from the mid to outer sections are further from equilibrium (Figs. 5 and 7).

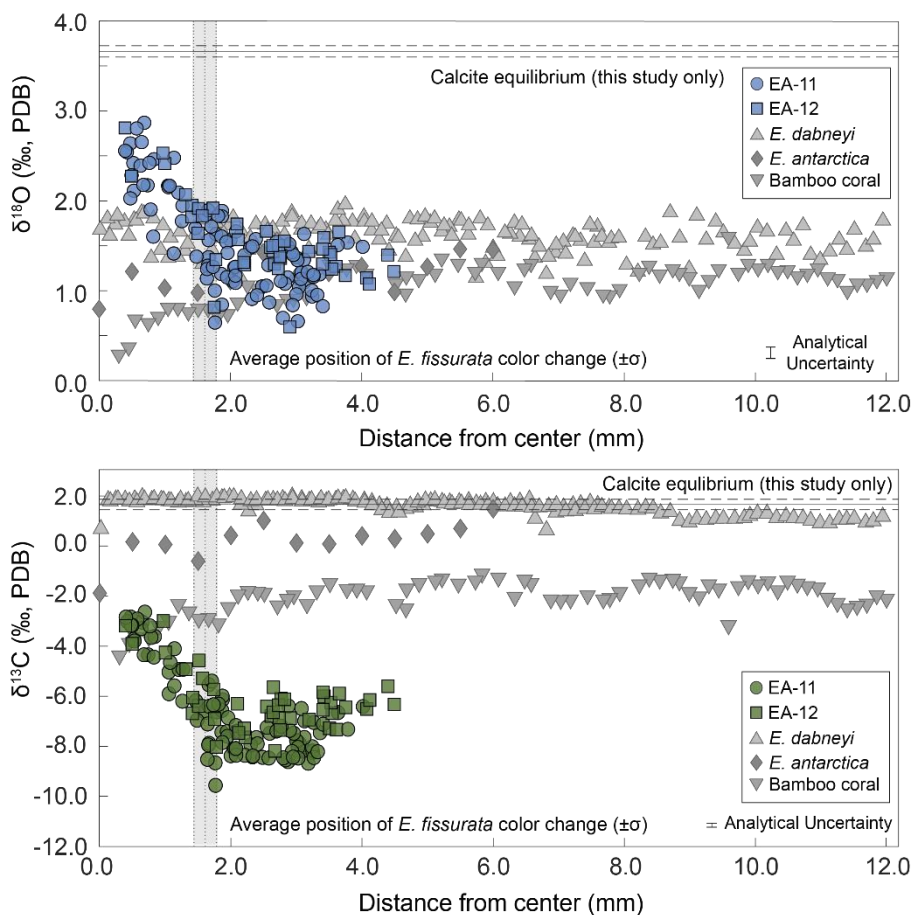


**Figure 7:** Oxygen (top) and carbon (bottom) stable isotope ratios by distance from the center of the coral. The values from this study are plotted by slice from each specimen as noted by the colored circles (EA-11) and squares (EA-12). The horizontal lines denote calculated ~~aragonite and~~ calcite equilibrium values for this study with corresponding uncertainty in dashed lines ( $\pm 1\sigma$ ). Vertical gray bars denote the average radius of the white coral center for *E. fissurata*, the width of the bar denoting  $\pm 1\sigma$ . Also included are additional coral data in a similar transect style. *E. dabneyi* is from Wissshak et al. (2009), *E. antarctica* is from Samperiz et al. (2020), and the bamboo coral data are from Hill et al. (2011). Regarding  $\delta^{18}\text{O}$ , the *E. antarctica* and bamboo coral seem to have a small decrease in the last few datapoints toward the center. Regarding  $\delta^{13}\text{C}$ , the same is true of each of the corals from other studies. This ~~contrast is opposite of what the increase~~ we observe in our corals. ~~We also note a much larger magnitude of change across the transect with no observable trend among coral slices (i.e., by distance from the coral tip), only the increase in isotopic values toward the white, center region of the corals.~~

#### 4.1 Evaluation of major $\delta^{18}\text{O}$ and $\delta^{13}\text{C}$ trends

Regarding large-scale isotopic trends from the tip to the base of each coral specimen, our results do not directly support those of Samperiz et al. (2020). Stable oxygen and carbon isotope analysis of *E. fissurata* supports an influence of vital effects on the skeletal geochemistry of this stylasterid species. Because little is known about the biocalcification mechanisms and processes of stylasterid corals, we discuss here any similarities to other coral records and present new insights. Fractionation towards lower isotopic ratios relative to equilibrium as well as a positive correlation between  $\delta^{18}\text{O}$  and  $\delta^{13}\text{C}$  values has been well documented among skeletal records generated from different classes of corals (e.g., Emiliani et al., 1978; Swart, 1983; McConnaughey, 1989a; Smith et al., 2000; Adkins et al., 2003; Hill et al., 2011; Samperiz et al., 2020; Stewart et al., 2020). In Figure 5, we compare new data from this study with several scleractinian and bamboo corals. Our data. The linear regression between *E. fissurata*  $\delta^{18}\text{O}$  and  $\delta^{13}\text{C}$  values exhibit very similar slopes to other deep-sea corals and fall within similar ranges of isotopic compositions. This supports that vital effects can have a similar influence on corals of different classes, and across different latitudinal and depth ranges. Unlike the scleractinian corals analyzed by Adkins et al. (2003), *E. fissurata* does not exhibit a “break” in the slope of the linear regression (Fig. 4). This is supported by the findings of Stewart et al. (2022) wherein boron isotopes revealed that stylasterids do not upregulate the pH of their internal calcifying fluids to enhance calcification, thus altering the linear relationship between isotope ratios. An unusual isotopic trend from the *E. fissurata* corals is the innermost values of each sample disc approaching equilibrium (Figs. 3, 5, and 7). This contrasts the findings of Samperiz et al. (2020) who measured the innermost portion of *E. antarctica* as furthest from isotopic equilibrium (Fig. 7; note that the equilibrium value in this figure is for this study only, however, the *E. antarctica* isotope ratios clearly decrease towards the coral center). Additionally, Hill et al. (2011) sampled bamboo corals across a transect which resulted in  $\delta^{18}\text{O}$  and  $\delta^{13}\text{C}$  values further from equilibrium in the center of the coral (Fig. 7). Results from Wisshak et al. (2009) can only partially support these works as they generated  $\delta^{13}\text{C}$  values from the center *E. dabneyi* that produced a single value from the innermost portion that was much lower than equilibrium (Fig. 7). Stable isotope ratios closer to equilibrium in the center of *E. fissurata* are the first of their kind for stylasterids and we posit that they imply lessening vital effects in this region because of slower calcification rates (McConnaughey, 1989b). Figure 7 also illustrates the wide range in isotopic variability exhibited by *E. fissurata* compared to the aragonitic *Erinna* and calcitic bamboo corals (Wisshak et al., 2009; Hill et al., 2011, respectively). The range in isotope values that trend toward equilibrium in the center of the coral could be a result of a unique calcification strategy that also leads to a lack of visible banded structure within *E. fissurata*.

Rapid calcification rates, and therefore prominent vital effects have been interpreted as the reason that *E. antarctica* growth tips exhibit some of the lowest  $\delta^{18}\text{O}$  and  $\delta^{13}\text{C}$  values when compared to main trunk and branch samples (Samperiz et al., 2020). Here, the most negative  $\delta^{18}\text{O}$  and  $\delta^{13}\text{C}$  values for EA-11 were measured on the slice closest to the tip, EA-11a, and the most positive  $\delta^{18}\text{O}$  and  $\delta^{13}\text{C}$  values were measured on a slice furthest from the tip, EA-11d (Fig. 4). Specimen EA-12 was

characterized by  $\delta^{18}\text{O}$  and  $\delta^{13}\text{C}$  minima nearest the tip (EA-12a), but the maximum isotope ratios were measured on different slices: the most positive  $\delta^{18}\text{O}$  was closer to the tip and the most positive  $\delta^{13}\text{C}$  was further away (Fig. 4 and Table 2). These observations, however, are not a direct comparison to measurements by Samperiz et al. (2020) for two reasons. First, the sampling scheme here was designed to exploit isotopic variability across a coral slice, thus considering calculated “bulk” values from each slice should provide more comparable value. However, our calculated bulk values do not exhibit any significant changes over the lengths of the corals; they all exhibit similar variance along their respective coral and are within error of each other (Fig. 4). This could be due to the second limitation on comparisons: we did not sample the true tips of the corals, but instead were ~1 cm below, possibly preventing us from sampling the most negative  $\delta^{18}\text{O}$  and  $\delta^{13}\text{C}$ , so we cannot truly compare growth tips. We are also uncertain of the lower extent of EA-11 and EA-12, as they were dredge collected, and could be missing a portion of the main trunk, possibly preventing us from sampling the most positive  $\delta^{18}\text{O}$  and  $\delta^{13}\text{C}$  (Fig. 2).

In their work, Samperiz et al. observed significant differences among stable isotopic compositions of carbonate sampled from different portions of a single specimen. Samples drilled from the main trunk and secondary branches exhibited higher  $\delta^{18}\text{O}$  and  $\delta^{13}\text{C}$  values (which were closer to seawater equilibrium) than the more distal growth tips. An observation evident in not only different genera of stylasterid corals, but also between calcite and aragonite mineralogies (Samperiz et al., 2020). Here, specimen EA-11 supported this observation as the most negative  $\delta^{18}\text{O}$  and  $\delta^{13}\text{C}$  values were measured on the slice closest to the tip, EA-11a, and the most positive  $\delta^{18}\text{O}$  and  $\delta^{13}\text{C}$  values were measured on a slice furthest from the tip, EA-11d (Fig. 4). Specimen EA-12 was characterized by  $\delta^{18}\text{O}$  and  $\delta^{13}\text{C}$  minima nearest the tip (EA-12a), but the maximum isotope ratios were measured on different slices: the most positive  $\delta^{18}\text{O}$  was closer to the tip and the most positive  $\delta^{13}\text{C}$  was further away (Fig. 4 and Table 2). These results neither completely support nor refute those of Samperiz et al. (2020). We posit that our sampling scheme hindered a full support from both corals analyzed here. For EA-12, we did not sample the main coral trunk, but rather just above it, targeting a region that exhibited isotopic variability in the corals from Samperiz et al. (2020) (Fig. 2). The sampling scheme here was designed to exploit any isotopic variability across a coral slice, thus considering the “bulk” values from each slice should provide a more comparable sampling strategy to Samperiz et al. (2020). However, our calculated bulk values do not exhibit any significant changes over the lengths of the corals (Fig. 4). This could be because we did not sample the true tips of the corals, but instead were ~1 cm below, possibly preventing us from sampling the most negative  $\delta^{18}\text{O}$  and  $\delta^{13}\text{C}$ . We are also uncertain of the lower extent of EA-11 and EA-12, as they were dredge collected, and could be missing a portion of the main trunk, possibly preventing us from sampling the most positive  $\delta^{18}\text{O}$  and  $\delta^{13}\text{C}$  (Fig. 2).

Another isotopic trend we consider here is that of the linear correlation between  $\delta^{18}\text{O}$  and  $\delta^{13}\text{C}$  values. Because these corals are living animals, and their biological functions affect the carbon and oxygen pools from which they calcify, we anticipated that the resulting  $\delta^{18}\text{O}$  and  $\delta^{13}\text{C}$  records would be positively correlated and offset to more negative values than calculated equilibrium (Emiliani et al., 1978; Swart, 1983; McConnaughey, 1989a; Smith et al., 2000; Adkins et al., 2003; Hill et al., 2011; Samperiz et al., 2020; Stewart et al., 2020). In Figure 5, we compare the data from this study with several scleractinian

and bamboo corals (class Anthozoa). Our data exhibit very similar slopes to other deep sea corals and fall within similar ranges of isotopic compositions. This supports that vital effects can have a similar influence on corals of different classes, and across different latitudinal and depth ranges. An additional influence on skeletal  $\delta^{18}\text{O}$  and  $\delta^{13}\text{C}$  values of stylasterid corals is carbonate mineralogy. It has been widely known that fractionation of stable oxygen and carbon isotopes occurs between carbonate and seawater, the magnitude of which is different for aragonite and calcite (e.g., O'Neil et al., 1969; Grossman and Ku, 1986; Swart, 1983; Romanek et al., 1992). This has been observed in laboratory settings, as well as organisms that precipitate carbonate shells or skeletons (Romanek et al., 1992; Lécuyer et al., 2012; Samperiz et al., 2020, respectively). In addition to taxonomical organization, mineralogical content has recently become a common method by which to categorize specimens when analyzing skeletal geochemistry (Stewart et al., 2020; Samperiz et al., 2020; Stewart et al., 2022; Kershaw et al., 2023). The *E. fissurata* here were determined to be mixed mineralogy; mainly calcite with some aragonite, and likely a slightly greater proportion of aragonite in the white center compared to the pink outer region (Fig. S3 in the Supplement; Table 3). The mineralogy data reported in Table 3 are from specimens EA-13 and EA-14 which, although were collected from the same dredges, are not the corals analyzed for stable isotope values, and therefore might be characterized by slightly different calcite and aragonite proportions. With such apparent mineralogical variability among the *Errina* genus (see Fig. 6; Cairns and Macintyre, 1992), it would be prudent to assume some variability among individuals within a species. The sample that was analyzed for both stable isotopes and mineralogy, EA-11d, was scanned for XRD over the entire slice as a bulk measurement, as well as two outer pink samples and one white center sample (see Fig. 3 for EA-11d image; Fig. S3 in the Supplement). The bulk sample would be most comparable to the bulk mineralogy data reported in the literature, but the subsamples of coral color bands are the first of their kind. The peak intensities from the coral color bands show some differences between the pink and white, however, the scan of the “right side” pink band may have incorporated some of the white center as the coral did not produce completely straight demarcations (see EA-11d in Figs. 2 and 3). This work presents the first skeletal stable isotope values collected from mixed mineralogy stylasterids, and further, the first stylasterid mineralogical data obtained by methods other than bulk sample analysis. Despite mixed mineralogy, the *E. fissurata*  $\delta^{18}\text{O}$  and  $\delta^{13}\text{C}$  values align well in isotope space with other calcitic stylasterids; they are further offset from isotope equilibrium than their aragonitic counterparts along the  $\delta^{13}\text{C}$  axis, but within range of the aragonitic  $\delta^{18}\text{O}$  values (Fig. 6). We also compare our corals to the deep sea stylasterids compiled by Samperiz et al. (2020) and Wisshak et al. (2009) (Fig. 6). Samperiz et al. (2020) observed that calcitic specimens exhibited  $\delta^{18}\text{O}$  and  $\delta^{13}\text{C}$  values further from equilibrium (i.e., more negative) compared to aragonitic corals. Because our calculated equilibrium  $\delta^{18}\text{O}$  and  $\delta^{13}\text{C}$  values were higher for aragonite than calcite, our data relative to aragonite equilibrium are further offset, contradicting the observation made by Samperiz et al. (2020). However, our data relative to calcite equilibrium exhibit overlaps with both calcitic specimens and some aragonite *Errina* data points as well (Fig. 6, Sect. 4.2.3). Thus far our data fit in well with established  $\delta^{18}\text{O}$  and  $\delta^{13}\text{C}$  records from other deep sea stylasterids, scleractinians, and bamboo corals. Our data are distinguished when we examine the heterogeneous  $\delta^{18}\text{O}$  and  $\delta^{13}\text{C}$  values across a coral slice.



We compare our  $\delta^{18}\text{O}$  and  $\delta^{13}\text{C}$  results to those of other azooxanthellate, deep-sea stylasterid and bamboo corals sampled in a similar manner, i.e., across growth bands, perpendicular to the growth axis. The range of  $\delta^{18}\text{O}$  values for EA 11 and EA 12 is 2.27 ‰, larger than the range for the *E. dabneyi* (-0.8 ‰; Wisshak et al., 2009), *E. antarctica* (-0.6 ‰; Samperiz et al., 2020), and the bamboo coral (-1 ‰; Hill et al., 2011) (Fig. 7). Similarly, greater heterogeneity is evident in the range of  $\delta^{13}\text{C}$  values exhibited by EA 11 and EA 12 (6.92 ‰) compared to *E. dabneyi* (-1.4 ‰), *E. antarctica* (-3 ‰), and the bamboo coral (-3.5 ‰) (Fig. 7). This contradicts results of Stewart et al. (2020) wherein the authors find that stylasterid corals of mixed mineralogy exhibit less variability compared to purely aragonitic scleractinians and stylasterids. We have evidence for a mixed calcite and aragonite mineralogy in the corals presented here (Sect. 4.2.3), but they are characterized by the largest stable isotope variability. This could be an artifact of sampling scheme between our study and Stewart et al. (2020), as our method was designed to amplify spatial variability in stable isotopic compositions across the coral slices. The increased internal variability could also be a species specific effect such that the calcification pattern for *E. fissurata* imparts stronger vital effects in the mid to outer coral regions compared to center. Spatially variable vital effects have been observed in many deep-sea corals, and departures of at least 2 ‰ in  $\delta^{18}\text{O}$  have been recorded by *D. cristagalli* (Smith et al., 2002; Adkins et al., 2003). To test if the  $\delta^{18}\text{O}$  variability in our corals represents an environmental signal, we use the stylasterid temperature calibration from Samperiz et al. (2020) and calculate the temperature change to be up to -7 °C across each coral slice and -10 °C along the vertical section of EA 11d. Such temperature changes are too large for the western Ross Sea over the lifespan of a single coral specimen (estimated to be ~200–400 years based on growth rate estimates for this species by King et al. (2018)). In Figure 7, we are also able to compare the trends of our  $\delta^{18}\text{O}$  and  $\delta^{13}\text{C}$  values to those of *E. dabneyi*, *E. antarctica*, and bamboo coral specimens across their surfaces, perpendicular to the growth axis. Our stylasterids demonstrate a very clear and large magnitude shift to higher  $\delta^{18}\text{O}$  and  $\delta^{13}\text{C}$  values toward the center of the coral slice (Fig. 7). This is opposite to the trend exhibited by the *E. antarctica* and bamboo coral  $\delta^{18}\text{O}$  values, and all three corals'  $\delta^{13}\text{C}$  values. Because the three external corals were sampled following visual growth banding, we posit that there is a difference between the two main growth styles (calcification) that cause the disparity in the central  $\delta^{18}\text{O}$  and  $\delta^{13}\text{C}$  values related to vital effects.

## 4.2 Surveying maps of skeletal stable isotope composition: alternative mechanisms for high central $\delta^{18}\text{O}$ and $\delta^{13}\text{C}$ values

### 4.2.1 Organic contribution to outer skeletal portion

Stylasterid corals have been observed hosting other species including boring cyanobacteria, sponges, and gastropods, all of which could affect the isotopic composition of the coral skeleton (Puce et al., 2009; Braga-Henriques et al., 2010; Pica et al., 2015). The presence of [such organismssymbionts](#) could contribute metabolic carbon and/or oxygen to the pool from which the corals calcify, [similar to the metabolic effects of shallow-water coral symbionts \(e.g., McConnaughey, 1989a\)](#). Depending on the relationship of the [symbiontepiphyte](#), and if it is living near an active calcification site, isotopically light metabolic products could be incorporated into the coral carbonate, driving the outer portions of the coral to lower  $\delta^{18}\text{O}$  and  $\delta^{13}\text{C}$  ([Epstein et al., 1951](#)). There have been direct observations of barnacles living on *E. fissurata* (Pica et al., 2015). For specimen EA-11, sections

with any obvious external growth or signs of hosting were avoided and only clean slices were selected for sampling. For EA-12, however, this coral was believed to be dead upon collection, and covered in possible organic growth/encrustation over time (Fig. 2). We posit that this material was not present at the time of coral calcification and therefore would not have altered the  $\delta^{18}\text{O}$  and  $\delta^{13}\text{C}$  values of the carbonate. The similarity in isotope trends between both specimens supports this hypothesis.

#### 4.2.2 Diagenetic influence on stable isotopic composition

Coral diagenesis can be described as a post-calcification alteration of carbonate geochemistry. Such processes could directly change the skeletal  $\delta^{18}\text{O}$  and  $\delta^{13}\text{C}$  values by removing or replacing the carbonate. Identifiable diagenetic features for stylasterid corals have been described by Black and Andrus (2009), including encrustation of foreign materials on the outer surface of the coral skeleton, microspar fabric and microbioclastic debris, abrasions, fragmentation, pitting, and bioerosion. These features are identifiable via scanning electron microscopy (SEM), but the authors found no impact on the  $\delta^{18}\text{O}$  and  $\delta^{13}\text{C}$  after analyzing fossil and modern corals (Black and Andrus, 2009). Work by Wisshak et al. (2009) has identified additional diagenetic impacts on stylasterid corals via micro-scale dissolution and re-precipitation. We were able to analyze *E. fissurata* live-collected specimens EA-22, EA-23, and EA-24 for physical signs of diagenesis. Although we did not image specimens EA-11 or EA-12, via SEM, but we were able to image other specimens the others were collected from the same dredges. We imaged slices of coral branches similar to the stable isotope sampling scheme and did not see any signs of the diagenetic effects described, except for possible secondary growth or recrystallization (Figs. S43 and S5 in the Supplement). Although we have identified evidence of secondary crystal growth, the scale is on the order of  $\sim 100\ \mu\text{m}$ . That size is 5 times smaller than the size of the drill bit used here, and therefore unlikely to have an impact on the  $\delta^{18}\text{O}$  and  $\delta^{13}\text{C}$  variability observed.

#### 4.2.3 Calcite versus aragonite mineralogy

With the XRD data presented here, there are multiple lines of evidence for mixed calcite and aragonite *E. fissurata* skeletons. This is important to consider because the mineral phase of carbonate can influence isotopic fractionation, as described above. Comparing  $\delta^{18}\text{O}$  and  $\delta^{13}\text{C}$  values from eight specimens of *Cheiloporidion pulvinatum* (five purely aragonite and three purely calcite) collected from the same location resulted in an average difference of  $\sim +1.4\ \text{‰}$   $\delta^{18}\text{O}$  and  $\sim +5.3\ \text{‰}$   $\delta^{13}\text{C}$ , the higher values being aragonite (Samperiz et al., 2020). Despite the quantitative XRD analyses being performed on corals not used for stable isotope measurements, we cannot eliminate mineralogy as a potential driver for the change in isotope composition toward the center of the corals. Stylasterid corals have been shown to precipitate their skeletons from calcite, aragonite, and both coexisting polymorphs (Cairns and Macintyre, 1992). Calcitic stylasterid corals have demonstrated significantly lower  $\delta^{18}\text{O}$  and  $\delta^{13}\text{C}$  values than aragonite stylasterids (Samperiz et al., 2020). As mentioned in a previous section, stylasterids have also

Coral	Sample Location	Aragonite	Calcite
EA-13 (Live)	Center <u>white</u>	23%	77%
	External <u>pink</u>	20%	80%
EA-14 (Dead)	Center <u>white</u>	30%	70%
	External <u>pink</u>	25%	75%

**Table 3:** Results for XRD mineralogical analysis of *E. fissurata*.

570 exhibited different levels of  $\delta^{18}\text{O}$  and  $\delta^{13}\text{C}$  variability within a single coral based on mineralogy (Stewart et al., 2020). Thus,  
mineralogy will have a significant impact on stable isotopic composition. The specimens in this study were not used for  
mineralogical analysis, but corals from the same dredges were. Using both XRD and false color imaging methods, we have  
identified that these corals are likely mixed mineralogy, and mostly calcitic (Table 3 and Fig. S4 in the Supplement). Two *E.*  
*fissurata* corals were sampled [here](#) (one modern and one dead) from both the center white, and outer pink regions. Each coral  
575 sample produced similar results of ~75 % calcite, and ~25 % aragonite (Table 3). ~~We consider that~~ There is, however, a small  
change in the percentage of ~~aragonite~~ calcite from the outer portions of both corals (~~75 % to 80 %~~) compared to the inner  
portions (~~70 % to 77 %~~) wherein they increase by magnitudes of 3 % (EA-13) and 5 % (EA-14) towards the center. These are  
not large changes and may not produce the magnitude of isotopic differences observed between pure aragonite and calcite by  
Samperiz et al. (2020). However, these are the first  $\delta^{18}\text{O}$  and  $\delta^{13}\text{C}$  records from stylasterids of mixed mineralogy so we must  
580 consider a mineralogical driver and pursue it further as an avenue to understand *E. fissurata* biocalcification and use as a  
paleoceanographic archive. However, the changes are small, and we posit that although calcitic stylasterids demonstrate lower  
skeletal  $\delta^{18}\text{O}$  and  $\delta^{13}\text{C}$  values compared to aragonite, the mineralogical difference is likely not enough to be driving the  $\delta^{18}\text{O}$   
and  $\delta^{13}\text{C}$  patterns here (Fig. 3).

#### 4.3 Hypothesized large-scale calcification model for *E. fissurata*

585 To further investigate the possibility of vital effects leading to ~~The most parsimonious explanation for the~~ specimen-scale  
differences in  $\delta^{18}\text{O}$  and  $\delta^{13}\text{C}$  values, we posit ~~is that the coral~~ *E. fissurata* calcifies in a way that magnifies the vital effects in  
the outer region compared to the center. In order to grow dendritically, the most intuitive growth model for corals such as our  
stylasterids holds that the center of each branch extends axially faster than each branch thickens radially. Thus, the kinetic  
effects would be most apparent in the center of each coral slice and lessen towards the outer edges, resulting in  $\delta^{18}\text{O}$  and  $\delta^{13}\text{C}$   
590 values that would therefore approach equilibrium toward the edges of each isotope map. Many marine calcifying organisms  
(e.g., mollusks and corals) follow the Von Bertalanffy growth model wherein their calcification rate ontogenetically  
decreases, and we posited that this model also applied to the horizontal extension of stylasterids as they prioritize vertical  
growth (Ralph and Maxwell, 1977; Emiliani et al., 1978; Berkman, 1990; Philipp et al., 2005; Román-González et al., 2017).  
Such a coral growth model is supported by observations from Fallon et al. (2014) wherein a cold water scleractinian coral  
595 demonstrated growth similar to stacking cones with a fast growing tip. This structure is also supported by isotopic records of  
other stylasterids and bamboo corals which were all characterized by low isotopic values at the regions of most rapid growth  
(Wisshak et al., 2009; Samperiz et al., 2020; Hill et al., 2011).

To better understand our resulting trends, we created models that reflect simplified calcification scenarios of constant, decreasing, and increasing radial extension with time. The model calculations were based on an idealized coral slice of  $n$  rings with radii,  $r_{n+1}$ , an initial growth inner circle of radius,  $r_1$ , and the extension rate represented by the change in radius,  $\Delta r$ , between each ring (Fig. 8). We set each model to run for 100 years and examined the rate of change of coral area as a proxy for calcification rate in each scenario. Whereas few studies have determined vertical growth rates of deep-sea stlyasterid corals (Stratford et al., 2001; Chong and Stratford, 2002; Miller et al., 2004; Wisshak et al., 2009; King et al., 2018), their radial extension rates remain largely unknown. Therefore, we employed a range of radial growth rates reported for live-collected bamboo corals living at a depth of 1000–1700 m (Thresher et al., 2011). The bamboo corals were reported to grow from 0.01–0.12 mm  $y^{-1}$ ; therefore, our constant radial extension scenario was characterized by the median 0.065 mm  $y^{-1}$  (Fig. 9a–c). The decreasing radial extension scenario was initially set to the maximum extension rate of 0.12 mm  $y^{-1}$  that decreased linearly by 0.0011 mm  $y^{-2}$  until the minimum growth rate of 0.01 mm  $y^{-1}$  was reached at 100 years (Fig. 9d–f). For the increasing radial extension scenario, the opposite was set, an initial radial extension rate of the minimum 0.01 mm  $y^{-1}$  and a linear increase at a rate of 0.0011 mm  $y^{-2}$  until 0.12 mm  $y^{-1}$  at 100 years (Fig. 9g–i).

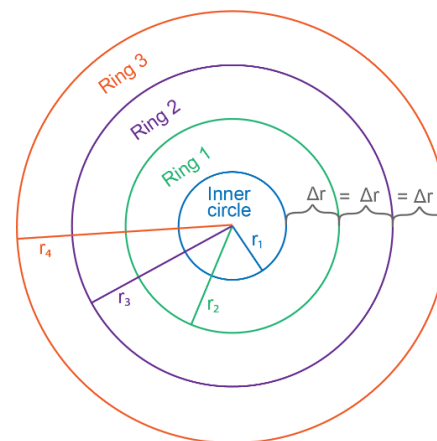


**Figure 8:** Coral slice schematic used for calcification models. In this simplified model, growth begins with the inner circle of radius  $r_1$ . Each growth increment is noted by a new ring, Ring  $n$ , with a radius,  $r_{n+1}$ . In this case, the change in radius between each ring,  $\Delta r$ , is equal representing the constant radial extension model. The  $\Delta r$  becomes larger or smaller with each ring for the increasing and decreasing growth scenarios, respectively.

We observe stronger vital effects toward the outer edges of the *E. fissurata* coral slicesurfaces and interpret this as increased calcification rate along the outer edges. To test if this growth scenario likely represents our stable isotope maps, we defined changes in calcification rate as the two-dimensional changes in coral area with time. We then compared the resulting models to the changes in stable isotope values across each coral slice (assuming no change in the ambient seawater values during the time of precipitation). In the case of the constant radial extension, the growth rings are evenly spaced, leading to a steady increase of horizontal area between the rings with time (Fig. 9a and b). Constant radial extension refers to constant change in area with time (Fig. 9c). Such a growth model would result in stable isotope values to either be constant across the surface of

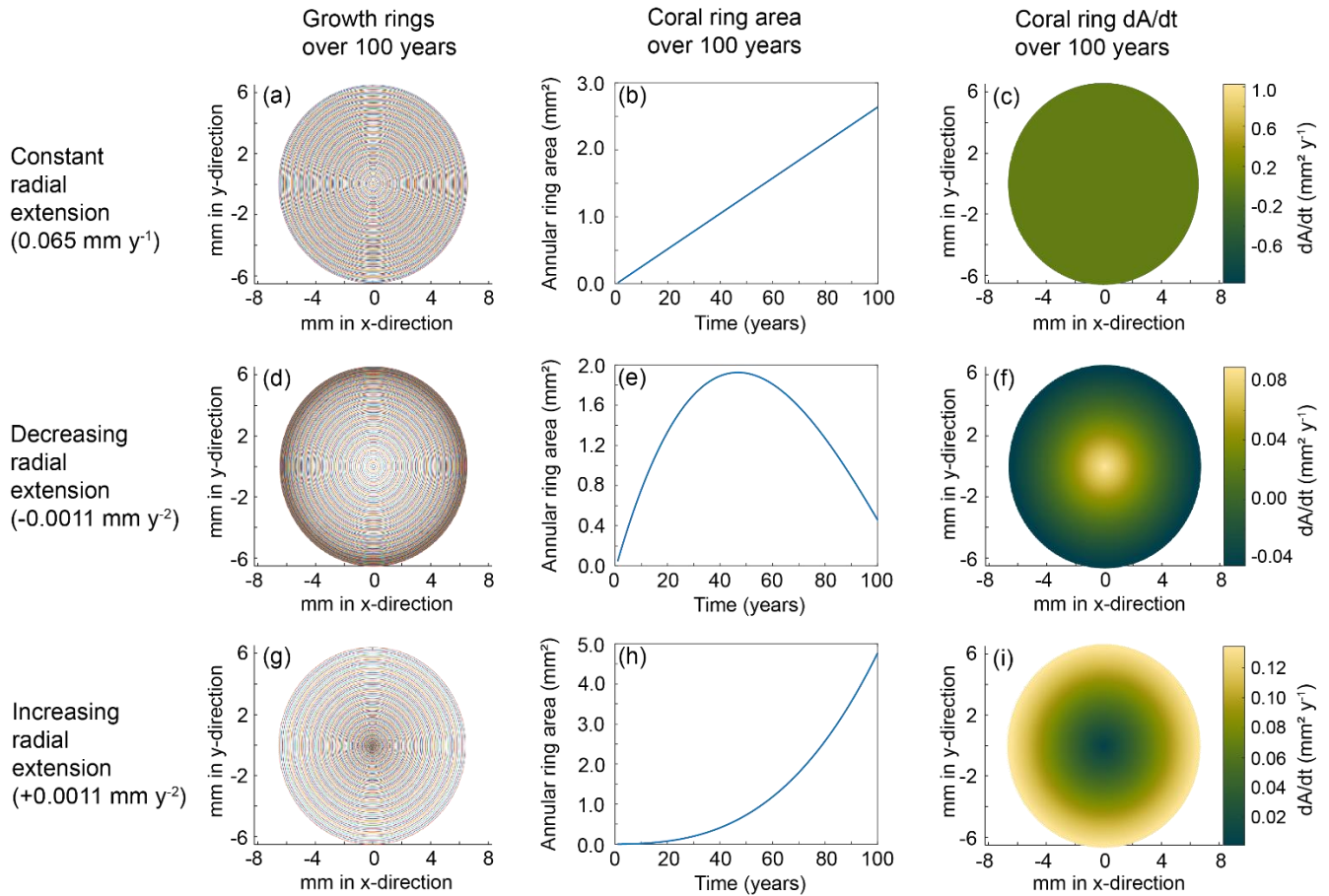


**Figure 9:** Coral calcification models for each scenario. The top row (a–c) depicts results from the constant radial extension model, the middle row (d–f) is the decreasing radial extension, and the bottom row (g–i) is the increasing radial extension model. The left column depicts the growth rings for each model after a run of 100 years. The middle column shows the change in area with each year of calcification. The right column shows the rate of change in coral area for each model. The corresponding color bars represent the magnitude of change.

625 the coral or record any changes that reflect seawater variability. Decreasing radial extension with time relates to decreasing  
 area with time (Fig. 9d–f). ~~We hypothesized decreasing radial extension to and would~~ be the most likely calcification pattern  
 as the available literature supports slowing growth with time among marine carbonates (Ralph and Maxwell, 1977; Emiliani  
 et al., 1978; Berkman, 1990; Philipp et al., 2005; Román-González et al., 2017). With ~~a~~ decreasing radial extension, the growth  
 bands become closer with time, causing the area to increase then decrease over the modeled 100-year span (Fig. 9d and e).  
 630 Therefore, the rate of change of area decreases toward the outer edges of the coral surface (Fig. 9f). ~~Because faster calcification~~  
~~results in stronger vital effects, and~~ the center of the coral would exhibit isotope values furthest from equilibrium. That is the  
 opposite of what we observed ~~with *E. fissurata*~~. The increasing radial extension scenario led to growth bands increasing  
 distance from each other, resulting in an exponential increase in area (Fig. 9g and h). The resulting calcification scheme (i.e.,

rate of change in area) would lead to stronger vital effects toward the outer edges of the coral surface and isotopic values closer to equilibrium in the center (Fig. 9i) as observed with *E. fissurata*. ~~This is what we observed.~~

If driven by calcification scheme, ~~¶~~the unique pattern presented here of the highest isotopic values in the center of the coral with lower values toward the mid and outer edge ~~rejects our hypothesis for calcification and is contradicted by previously published isotope records and growth models. The stable isotope maps instead supports a model of~~ rapid calcification toward the outer region and slower calcification in the center. Such a model, however, is not supported by previously mentioned growth habits of marine carbonates and would not be expected to result in dendritic corals. ~~Several studies involving scleractinian corals and octocorals (class Anthozoa whereas stylasterids are class Hydrozoa) have converged on similar two-stage calcification patterns. Using X-ray micro-computed tomography, Urushihara et al. (2016) were able to determine that the cold water octocoral, *Corallium konojoi* (~290 m water depth), calcifies by two processes: formation of sclerites (small aggregates of carbonate within the coenenchyme tissue surrounding polyps) and a combined sclerite/biomineralization process at the apical region where skeletogenic epithelium secretes carbonate. A similar growth strategy was observed using incubated octocorals, *Corallium rubrum* (~20 m water depth), and measuring uptake of isotopic tracers (Allemand and Benazet-Tambutte, 1996). The authors found that the red coral forms its axial skeleton via biomineralization from the skeletogenic epithelium, which contributes to its horizontal extension. At the apical region, spicules fuse with the skeleton for vertical extension (Allemand and Benazet-Tambutte, 1996). Additional isotopic labeling experiments involving the zooxanthellate scleractinian, *Porites porites* (~50 m water depth), identified “hot spots” of calcification wherein biomineralization was not uniform across the growing surface of the coral (Houlbrèque et al., 2009). The authors attributed the heterogeneous calcification to an uneven distribution of extracellular calcifying fluid within the coral (Houlbrèque et al., 2009). The scleractinian calcification patterns described here are not a direct analog for our *E. fissurata* growth, however, To reconcile these contradictions, we explore calcification strategies that invokes uneven, or two-step biomineralization to could account for the spatial distribution of vital effects observed in our coral isotope maps.~~

A growth model of shallow water staghorn coral (*Acropora cervicornis*) over daily to yearly timescales best-reconciles our data (Gladfelter 1982, 1983, 1984). The Gladfelter model includes two main phases: rapid extension by randomly oriented crystals that develop the main skeletal framework, followed by infilling and strengthening of the skeleton along the entire growth axis (Gladfelter, 1982). Gladfelter (1983) observed that the initial framework growth was largely around the mid and outer regions of the corallite and the infilling occurred later in the center. We posit that the basic premise of this model (rapid initial growth followed by slower calcification) describes the coral growth presented here. The lower isotopic values toward the outer edge signify enhanced kinetic fractionation from the rapid growth. The center region of the coral calcifies at a slower rate; thus, kinetic fractionation is reduced resulting in higher isotopic values closer to equilibrium. We acknowledge that the Gladfelter growth model employs fusiform crystals setting a foundation upon which bundles of aragonite crystals grow, and we are not able to determine that scale of calcification here ~~do not suggest that the same crystal structures are apparent here.~~

We instead ~~hypothesize~~ posit that because of our consistent spatial isotopic discrepancies, and our contrast to previous stylasterid works, there must be a heterogeneous growth structure for *E. fissurata* not previously described for stylasterids, and the growth described by Gladfelter (1983) does this. ~~Our unique sampling scheme allowed for the resolution necessary to improve our understanding of the formation of a valuable paleoceanographic archive.~~

670 A final consideration for growth mechanisms driving the  $\delta^{18}\text{O}$  and  $\delta^{13}\text{C}$  trends in *E. fissurata* is that of the internal structures described for stylasterids. The stylasterid *Errina (Errina) labiata* was originally described by Moseley (1878). Internal, decalcified structures of *Errina* were described in this work including the coenosarcal mesh, which is a network of small canals just below the coral surface that increased in size and distance from each other deeper into the coral (Moseley, 1878). Wisshak et al. (2009) also observed these structures in their analysis of *E. dabneyi* microstructures. Vacuum-resin-embedded and

675 decalcified coral branches were observed to have very dense meshwork of canals near the outer surface of the corals which became wider, deeper inside (Wisshak et al., 2009). Puce et al. (2012) employed volume rendering methods using X-ray computed microtomography to identify microstructures of *Distichopora* specimens. This work agreed with the canal networks that are small near the surface of the coral and larger inside (Puce et al., 2012). Combined, these works support an uneven calcification mechanism for these few stylasterids that could also apply to *E. fissurata*. The small, densely packed meshwork

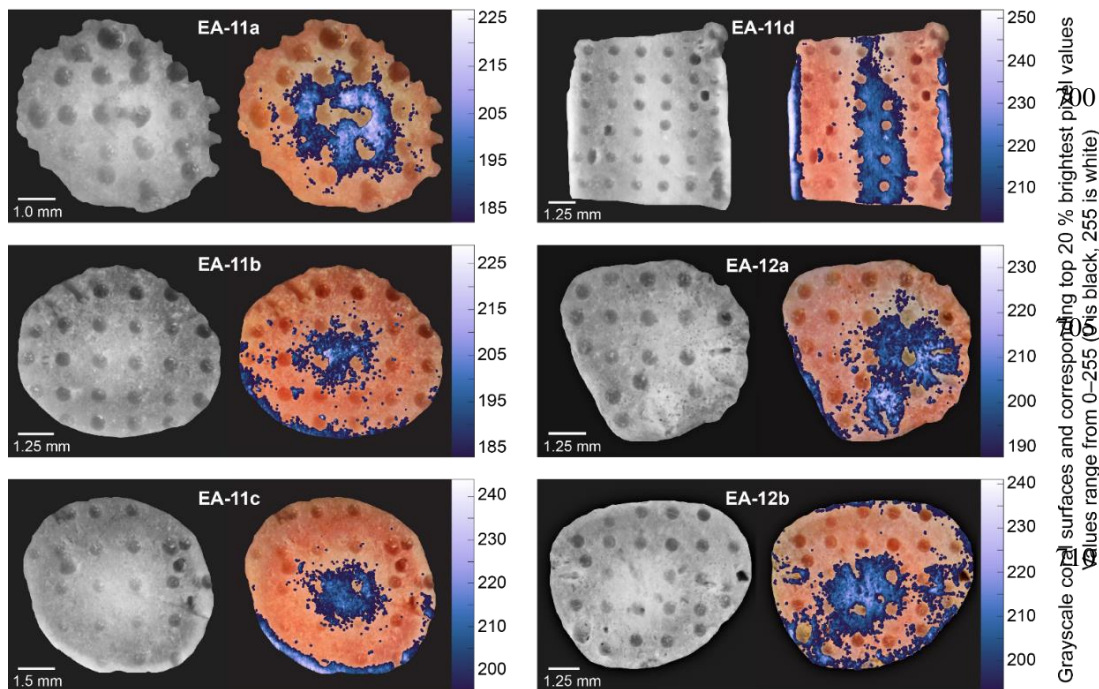
680 near the outer edges of the coral surface would have much more surface area than the larger, less dense canals in the coral interior. Therefore, the outer regions would require faster calcification rates to keep up growth of the entire coral colony. This uneven rate of calcification would impose vital effects in the outer regions of *E. fissurata* if a similar growth pattern were occurring, leaving the center region closest to isotopic equilibrium.

#### 4.4 Considerations for paleoceanographic reconstructions

685 The definitive trend of increasing isotopic values toward the inner, white section of the coral supports that this is the ideal region of the coral from which to sample *E. fissurata* for paleotemperature reconstructions. Because the higher values are located nearest the white section of the coral and not the geometric center, we converted the images of each slice to grayscale (Fig. 10). This allowed us to find the whitest pixels and quantitatively determine the most ideal location for sampling. With the exception of the light outer edges, the sample holes that were at least 75 % surrounded by the whitest pixels were selected

690 for temperature reconstructions (Fig. 10). These  $\delta^{18}\text{O}$  values were averaged for each coral slice and, in the absence of a mixed mineralogy  $\delta^{18}\text{O}$  temperature calibration for stylasterids, we use the temperature calibration equation from Samperiz et al. (2020). This equation was established for 100% aragonite stylasterid corals and it is unclear if this is appropriate for our mixed calcite and aragonite *E. fissurata*. ~~were used with the stylasterid temperature calibration from Samperiz et al. (2020).~~

695 Additionally, the  $\delta^{18}\text{O}$  average for each entire slice was calculated to determine a “bulk” value that would represent a common sampling method of drilling across the growth axis. The bulk  $\delta^{18}\text{O}$  values were also calibrated to temperature and the results are illustrated in Fig. 10 (Table S3 in the Supplement). Note that for slice EA-11d that consists of a vertical face rather than horizontal,  $\delta^{18}\text{O}$  values were only combined for the same distance from the coral tip.



Although both the “central” and “bulk” temperature records are higher than current ocean temperatures of a similar depth, the center values are significantly different from bulk measurements and are closer to the true environmental signal (Fig. 11). We compared the center and bulk temperature records using the Student’s t-Test to determine

Grayscale coral surfaces and corresponding top 20% brightest pixel values range from 0–255 (0 is black, 255 is white)

**Figure 10:** Compilation of grayscale images and corresponding brightest pixels (highest 20 %) over each coral slice. The colors correspond to the grayscale pixel value (higher on the scale bar denotes a whiter pixel). The sample holes surrounded by at least ~75 % of bright pixels were used to calculate representative  $\delta^{18}\text{O}$  values for each slice for temperature calibration (Table S3 in the Supplement).

whether the difference between the means is significant or occurred by chance (from variability). We used a paired t-Test to compare center and bulk temperatures from the same distance from the tip where available. With a p-value of  $6.61 \times 10^{-6}$ , the difference between center and bulk temperatures is very unlikely to have occurred by chance (Table S4 in the Supplement).

720 This analysis, however, assumes no environmental change over the lifespan of the corals. To account for possible seawater changes and more accurately reflect the samples that would be targeted for temperature reconstructions, we also tested individual temperatures across each slice (rather than the averages used in Fig. 11). The unpaired t-Test required at least two temperature values that were sampled from the white center and the pink outer regions for at least one degree of freedom. This was met by four coral slices, EA-11a, EA-11b, EA-11d (63.55 mm from the tip), and EA-12b; each test producing p-values  
725 less than 0.005 (Table S4 in the Supplement). These analyses show that we can conceive of no comparison within coral slices that show the same values between the center and bulk temperatures.



Figure 11 shows that detailed analysis of isotopic distributions through *E. fissurata* skeletons does not quite achieve samples representative of isotope equilibrium; but closer approach is possible. With the aid of computerized tomography (CT) scanning methods, perhaps density banding skeletal structures could be visualized, enabling even finer-scale samples. We posit that our prescribed sampling scheme for these corals, paired with CT-guided sampling, can yield robust paleotemperature records. Sampled as we have, with even distribution of samples over the surface of each disc as a goal, our reconstructed temperatures are higher than a likely environmental signal (Fig. 11). However, we have demonstrated that the center white region of these corals is less affected by vital effects and less likely altered after initial deposition. Therefore, we recommend sampling of the white center using more spatially precise micro-milling methods to target even smaller regions, thus minimizing the impact of vital effects. We also note that in calculating uncertainty associated with temperature calibrations, our center temperature errors are likely underestimated as they rely largely on analytical uncertainty. However, our calculation of temperatures from bulk data includes high spatial standard deviations; more precise sampling would yield more precise temperature estimates. Thus, a targeted milling approach would likely reflect a more accurate uncertainty estimate on the temperature as well. Additionally, CT scanning that reveals coral growth structures, such as Puce et al. (2011), would allow an even closer approach to accurate paleoceanographic reconstructions. Such combined methods would allow for extremely targeted sampling considering both the growth structure and biomineralization methods to inform sampling efforts to allow closer approach to equilibrium and better accuracy of paleotemperature reconstructions using *Errina* corals.

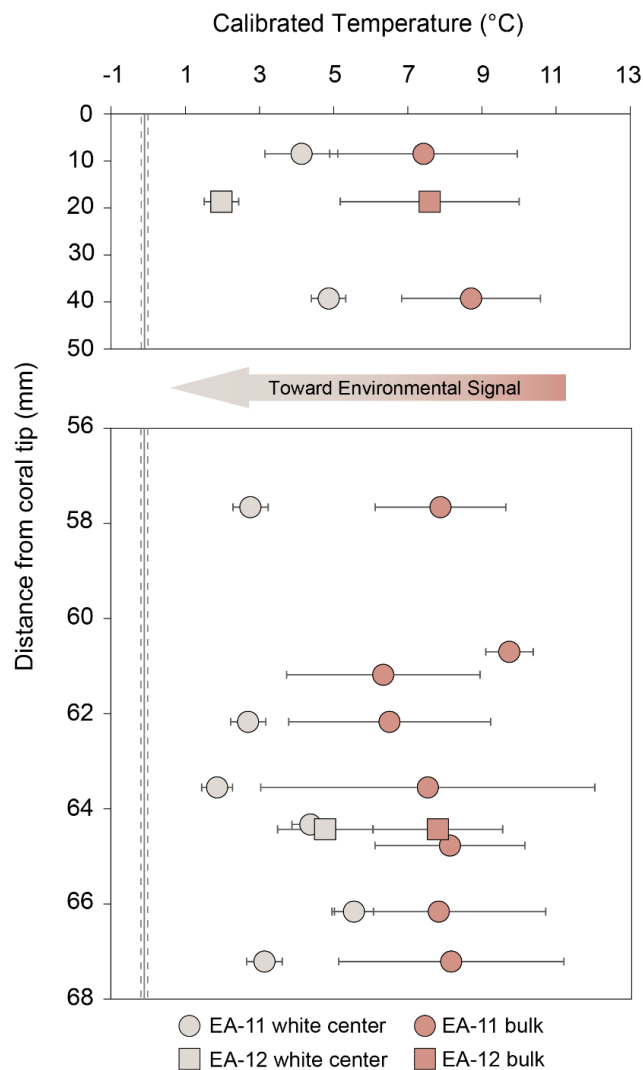


**Figure 11:** Temperature calibration using the equation from Samperiz et al. (2020) [for aragonite stylasterid corals](#). Light colored points denote temperatures using the  $\delta^{18}\text{O}$  values from the white centers of each slice, whereas the darker, peach color denote a “bulk” measurement. The bulk is calculated using the average  $\delta^{18}\text{O}$  of the entire slice, similar to a value that would be measured from a sample collected via drilling into the side of a coral specimen. Error bars are based on standard deviation of three or more averaged samples. The error bars for less than three samples are based on the analytical error propagation (Table S3 in the Supplement).

## 5 Conclusions

The results presented here ~~provide the paleoceanographic community with~~ contribute to a new understanding of ~~the highly diverse family of stylasterid corals. In the case of *E. fissurata*, a mixed mineralogy taxon, stable isotopic records provide geochemical details over a unique sampling resolution.~~ ~~the influence of vital effects on coral paleo-archives.~~ We have demonstrated that ~~*E. fissurata* deep-sea stylasterid corals~~ skeletons exhibit significant and variable vital effects ~~between different taxa~~ that obscure the environmental signal ~~of this potential paleoceanographic archive. In the case of *E. fissurata*, we are also able to provide and interpret isotope maps that guide future coral sampling efforts.~~ Lacking any visible banding structure, the specimens in this study benefitted from a gridded sampling scheme to determine the location of minimum influence from vital effects. Our skeletal  $\delta^{18}\text{O}$  and  $\delta^{13}\text{C}$  values exhibit an increasing trend toward seawater equilibrium near the center of the coral. This result contradicts growth structures hypothesized in the current body of literature based on observed stable isotopic trends ~~that have only focused on microsampling purely calcitic or purely aragonitic specimens~~ (Wisshak et al., 2009; Samperiz et al., 2020; Hill et al., 2011). ~~We posit that the observed trend in  $\delta^{18}\text{O}$  and  $\delta^{13}\text{C}$  values could be a result of changing mineralogical composition over the *E. fissurata* skeleton or a heterogeneous growth/calcification structure (or some combination of both).~~ ~~but supports a~~ Possible growth strategies include (i) a two-stage growth model ~~that describes~~ with a “hasty” initial lattice framework construction, followed by slower infilling to strengthen, and support the coral colony (Gladfelter, 1982, 1983) ~~or (ii) rapid calcification around the outer edges of the coral stem to construct the dense canal meshwork that is more sparse towards the center (Moseley, 1878; Wisshak et al., 2009; Puce et al., 2012).~~ We tested our interpretations that ~~t~~ ~~The  $\delta^{18}\text{O}$  values~~ samples from the center white region of the corals ~~were closest to equilibrium by calibrating them to seawater temperature using the paleotemperature equation developed by Samperiz et al. (2020) for aragonite stylasterids. These  $\delta^{18}\text{O}$  values~~ produced temperatures ~~records~~ significantly different than a bulk approach and were closest to nearby ocean temperatures. Thus, we recommend sampling this taxon along the center, white region where the carbonate geochemical record is closest to seawater equilibrium and an environmental isotopic signal. Further, we suggest initial CT scanning of corals to determine any hidden growth features, and micro milling sampling techniques to target the location of the most accurate record. Combined with ~~continued efforts to develop mixed mineralogy a new~~ stylasterid temperature calibration ~~(Samperiz et al., 2020)~~, we posit that accurate paleotemperature records can be reconstructed from deep-sea ~~*E. frina*~~ *fissurata* corals.

### Data availability

All data are available in the supplement.

## Author contributions

790 TMK and BER contributed to the conceptualization of the work. TMK developed sampling methods under the supervision of  
BER. [NPJ provided expertise on mineralogical analyses.](#) All authors contributed to formal analysis. TMK wrote the manuscript  
draft, with significant input from BER [and NPJ.](#) All authors approved the final version of the manuscript.

## Competing interests

The authors declare that they have no conflict of interest.

## 795 Acknowledgements

We thank the captain, crew, and scientific staff of the RV *Nathaniel B. Palmer* during the US Antarctic Program expedition  
NBP07-01 to the Ross Sea, Antarctica for their efforts in coral collection. We also thank Dr. Ernst Peebles for the use of  
laboratory space during coral sampling, and Drs. Jennifer Granneman and David Jones for guidance on both slicing the corals  
and initial setup of the MircoMill. [We also thank Dr. Lukasz Wojtas for providing XRD analysis at the University of South](#)  
800 [Florida and guidance during sample preparations.](#) During this project, TMK was funded through the Genshaft Family  
Dissertation Fellowship awarded by the University of South Florida as well as three endowed fellowships from the College of  
Marine Science: Carl Riggs Endowed Fellowship, George Lorton Fellowship in Marine Science, and the Abby Sallenger  
Memorial Award.

## 805 References

- Adkins, J. F., Cheng, H., Boyle, E. A., Druffel, E. R. M., and Edwards, R. L.: Deep-Sea Coral Evidence for Rapid Change in  
Ventilation of the Deep North Atlantic 15,400 Years Ago, *Science*, 280, 725–728,  
<https://doi.org/10.1126/science.280.5364.725>, 1998.
- Adkins, J. F., Boyle, E. A., Curry, W. B., and Lutringer, A.: Stable isotopes in deep-sea corals and a new mechanism for “vital  
810 effects,” *Geochim. Cosmochim. Ac.*, 67, 1129–1143, [https://doi.org/10.1016/S0016-7037\(02\)01203-6](https://doi.org/10.1016/S0016-7037(02)01203-6), 2003.
- Allemand, D. and Benazet-Tambutte, S.: Dynamics of calcification in the mediterranean red coral, *Corallium rubrum*  
(Linnaeus) (Cnidaria, Octocorallia), *J. Exp. Zool.*, 276, 270–278, [https://doi.org/10.1002/\(SICI\)1097-010X\(19961101\)276:4<270::AID-JEZ4>3.0.CO;2-L](https://doi.org/10.1002/(SICI)1097-010X(19961101)276:4<270::AID-JEZ4>3.0.CO;2-L), 1996.
- Andrews, A. H., Cordes, E. E., Mahoney, M. M., Munk, K., Coale, K. H., Cailliet, G. M., and Heifetz, J.: Age, growth and  
815 radiometric age validation of a deep-sea, habitat-forming gorgonian (*Primnoa resedaeformis*) from the Gulf of Alaska,  
*Hydrobiologia*, 471, 101–110, <https://doi.org/10.1023/A:1016501320206>, 2002.

- Arndt, J. E., Schenke, H. W., Jakobsson, M., Nitsche, F. O., Buys, G., Goleby, B., Rebesco, M., Bohoyo, F., Hong, J., Black, J., Greku, R., Udintsev, G., Barrios, F., Reynoso-Peralta, W., Taisei, M., and Wigley, R.: The International Bathymetric Chart of the Southern Ocean (IBCSO) Version 1.0-A new bathymetric compilation covering circum-Antarctic waters: IBCSO VERSION 1.0, *Geophys. Res. Lett.*, 40, 3111–3117, <https://doi.org/10.1002/grl.50413>, 2013.
- 820 Berkman, P. A.: The population biology of the Antarctic scallop, *Adamussium colbecki* (Smith 1902) at New Harbor, Ross Sea, in: *Antarctic Ecosystems*, edited by: Kerry, K.R. and Hempel, G., Springer, Berlin, Heidelberg, Germany, 281–288, [https://doi.org/10.1007/978-3-642-84074-6\\_32](https://doi.org/10.1007/978-3-642-84074-6_32), 1990.
- Black, H., and Andrus, C. F. T.: Taphonomy and diagenesis on the deep-sea hydrocoral *Styaster erubescens* fossils from the Charleston Bump, *Univ Alabama McNair J*, 12, 19-40, 2012.
- 825 Braga-Henriques A., Carreiro-Silva M., Porteiro F.M., de Matos V., Sampaio I., Ocaña O., and Avila S.P.: The association between a deep-sea gastropod *Pedicularia sicula* and its coral host *Errina dabneyi* in the Azores. *ICES J. Mar. Sci.* 68: 399–407, <http://doi.org/10.1093/icesjms/fsq066>, 2010.
- Burke, A. and Robinson, L. F.: The Southern Ocean’s Role in Carbon Exchange During the Last Deglaciation, *Science*, 335, 557–561, <https://doi.org/10.1126/science.1208163>, 2012.
- 830 Cairns, S. D.: A generic revision of the Stylasterina (Coelenterata: Hydrozoa). Part 1, Description of the genera, *B. Mar. Sci.*, 33, 427-508, 1983a.
- Cairns, S. D.: Antarctic and Subantarctic Stylasterina (Coelenterata: Hydrozoa), in: *Biology of the Antarctic Seas XIII*, vol. 38, edited by: Kornicker, S., American Geophysical Union, Washington, D. C., USA, 61–164, 1983b.
- 835 Cairns, S. D.: A generic revision of the Stylasteridae (Coelenterata: Hydrozoa). (Coelenterata: Hydrozoa). Part 3, Keys to the genera, *B. Mar. Sci.*, 49, 538-545, 1991.
- Cairns, S. D.: Worldwide distribution of the Stylasteridae (Cnidaria: Hydrozoa), *Sci. Mar.*, 56, 125–130, 1992.
- [Cairns, S. D.: Global Diversity of the Stylasteridae \(Cnidaria: Hydrozoa: Athecatae\), PLoS ONE, 6, e21670, https://doi.org/10.1371/journal.pone.0021670, 2011.](https://doi.org/10.1371/journal.pone.0021670)
- 840 Cairns, S. D. and Macintyre, I. G.: Phylogenetic Implications of Calcium Carbonate Mineralogy in the Stylasteridae (Cnidaria: Hydrozoa), *PALAIOS*, 7, 96-107, <https://doi.org/10.2307/3514799>, 1992.
- Chen, S., Gagnon, A. C., and Adkins, J. F.: Carbonic anhydrase, coral calcification and a new model of stable isotope vital effects, *Geochim. Cosmochim. Ac.*, 236, 179–197, <https://doi.org/10.1016/j.gca.2018.02.032>, 2018.
- Chen, T., Robinson, L. F., Burke, A., Claxton, L., Hain, M. P., Li, T., Rae, J. W. B., Stewart, J., Knowles, T. D. J., Fornari, D. J., and Harpp, K. S.: Persistently well-ventilated intermediate-depth ocean through the last deglaciation, *Nat. Geosci.*, <https://doi.org/10.1038/s41561-020-0638-6>, 2020.
- 845 Chong, A. K., and Stratford, P.: Underwater digital stereo-observation technique for red hydrocoral study. *Photogramm. Eng. Rem. S.*, 68(7), 745–752, 2002.
- Druffel, E. R. M.: Geochemistry of corals: Proxies of past ocean chemistry, ocean circulation, and climate, *P. Natl. Acad. Sci.*, 94, 8354–8361, <https://doi.org/10.1073/pnas.94.16.8354>, 1997.
- 850

- Druffel, E. R. M., King, L. L., Belostock, R. A., and Buesseler, K. O.: Growth rate of a deep-sea coral using  $^{210}\text{Pb}$  and other isotopes, *Geochim. Cosmochim. Ac.*, 54, 1493–1499, [https://doi.org/10.1016/0016-7037\(90\)90174-J](https://doi.org/10.1016/0016-7037(90)90174-J), 1990.
- Emiliani, C.: Pleistocene temperatures, *J. Geol.*, 63, 538–578, <https://doi.org/10.1086/626295>, 1955.
- 855 Emiliani, C., Hudson, J. H., Shinn, E. A., and George, R. Y.: Oxygen and carbon isotopic growth record in a reef coral from the Florida Keys and a deep-sea coral from Blake Plateau, *Science*, 202, 627–629, <https://doi.org/10.1126/science.202.4368.627>, 1978.
- Epstein, S., Buchsbaum, R., Lowenstam, H., and Urey, H. C.: Carbonate-water isotopic temperature scale, *Geol. Soc. Am. Bull.*, 62, 417–426, [https://doi.org/10.1130/0016-7606\(1951\)62\[417:CITS\]2.0.CO;2](https://doi.org/10.1130/0016-7606(1951)62[417:CITS]2.0.CO;2), 1951.
- 860 Epstein, S., Buchsbaum, R., Lowenstam, H., and Urey, H. C.: Revised carbonate-water isotopic temperature scale, *Bull. Geol. Soc. Am.*, 64, 1315–1326, [https://doi.org/10.1130/0016-7606\(1953\)64\[1315:RCITS\]2.0.CO;2](https://doi.org/10.1130/0016-7606(1953)64[1315:RCITS]2.0.CO;2), 1953.
- Fallon, S. J., Thresher, R. E., and Adkins, J.: Age and growth of the cold-water scleractinian *Solenosmilia variabilis* and its reef on SW Pacific seamounts, *Coral Reefs*, 33, 31–38, <https://doi.org/10.1007/s00338-013-1097-y>, 2014.
- Gerrish, L., Fretwell, P., & Cooper, P., High resolution vector polylines of the Antarctic coastline (7.5), UK Polar Data Centre, Natural Environment Research Council, UK Research & Innovation [Basemap] <https://doi.org/10.5285/bc71347d-298a-4df3-88b0-cb9a908db166>, 2022.
- 865 Gladfelter, E. H.: Skeletal development in *Acropora cervicornis*: I. Patterns of calcium carbonate accretion in the axial corallite, *Coral Reefs*, 1, 45–51, <https://doi.org/10.1007/BF00286539>, 1982.
- Gladfelter, E. H.: Skeletal Development in *Acropora cervicornis*: II. Diel patterns of calcium carbonate accretion, *Coral Reefs*, 2, 91–100, <https://doi.org/10.1007/BF02395279>, 1983.
- 870 Gladfelter, E. H.: Skeletal Development in *Acropora cervicornis*: III. A comparison of monthly rates of linear extension and calcium carbonate accretion measured over a year, *Coral Reefs*, 3, 51–57, <https://doi.org/10.1007/BF00306140>, 1984.
- Gordon, A.: Calibrated Hydrographic Data acquired with a CTD in the Ross Sea during the Nathaniel B. Palmer expedition NBP0302 (2003), Interdisciplinary Earth Data Alliance [CTD/Rosette], <http://doi.org/10.1594/IEDA/317291>, 2016.
- Gordon, A. L., Orsi, A. H., Muench, R., Huber, B. A., Zambianchi, E., and Visbeck, M.: Western Ross Sea continental slope gravity currents, *Deep-Sea Res. Pt. II*, 56, 796–817, <https://doi.org/10.1016/j.dsr2.2008.10.037>, 2009.
- 875 Griffin, S. and Druffel, E. R. M.: Sources of Carbon to Deep-Sea Corals, *Radiocarbon*, 31, 533–543, <https://doi.org/10.1017/S0033822200012121>, 1989.
- Grossman, E. L. and Ku, T.-L.: Oxygen and carbon isotope fractionation in biogenic aragonite: temperature effects, *Chem. Geol. (Isotope Geoscience Section)*, 59, 59-74, [https://doi.org/10.1016/0168-9622\(86\)90057-6](https://doi.org/10.1016/0168-9622(86)90057-6), 1986.
- 880 Heikoop, J. M., Dunn, J. J., Risk, M. J., Schwarcz, H. P., McConnaughey, T. A., and Sandeman, I. M.: Separation of kinetic and metabolic isotope effects in carbon-13 records preserved in reef coral skeletons, *Geochim. Cosmochim. Ac.*, 64, 975–987, [https://doi.org/10.1016/S0016-7037\(99\)00363-4](https://doi.org/10.1016/S0016-7037(99)00363-4), 2000.
- Hill, T. M., Spero, H. J., Guilderson, T., LaVigne, M., Clague, D., Macalello, S., and Jang, N.: Temperature and vital effect controls on bamboo coral (*Isididae*) isotope geochemistry: A test of the “lines method”, *Geochem. Geophys. Geosy.*, 12, 14, <https://doi.org/10.1029/2010GC003443>, 2011.
- 885

- Houlbrèque, F., Meibom, A., Cuif, J.-P., Stolarski, J., Marrocchi, Y., Ferrier-Pagès, C., Domart-Coulon, I., and Dunbar, R. B.: Strontium-86 labeling experiments show spatially heterogeneous skeletal formation in the scleractinian coral *Porites porites*, *Geophys. Res. Lett.*, 36, L04604, <https://doi.org/10.1029/2008GL036782>, 2009.
- 890 Jacobs, S.: Calibrated Hydrographic Data from the Ross Sea acquired with a CTD during the Nathaniel B. Palmer expedition NBP0408 (2004), Interdisciplinary Earth Data Alliance [CTD/Rosette], <http://doi.org/10.1594/IEDA/307443>, 2015.
- Jacobs, S. S., Fairbanks, R. G., and Horibe, Y. G.: Origin and evolution of water masses near the Antarctic continental margin: Evidence from H218O/H216O ratios in seawater, in: *Antarctic Research Series*, vol. 43, edited by: Jacobs, S., American Geophysical Union, Washington, D. C., 59–85, <https://doi.org/10.1029/AR043p0059>, 1985.
- 895 Jacobs, S. S., Amos, A. F., and Bruchhausen, P. M.: Ross Sea oceanography and Antarctic Bottom Water formation, *Deep-Sea Res. and Oceanographic Abstracts*, 17, 935–962, [https://doi.org/10.1016/0011-7471\(70\)90046-X](https://doi.org/10.1016/0011-7471(70)90046-X), 1970.
- [Kershaw, J., Stewart, J. A., Strawson, I., de Carvalho Ferreira, M. L., Robinson, L. F., Hendry, K. R., Samperiz, A., Burk, A., Rae, J. W., Day, R. D., and Etnoyer, P. J.: Ba/Ca of stylasterid coral skeletons records dissolved seawater barium concentrations, \*Chemical Geology\*, 662, p. 121355, <https://doi.org/10.1016/j.chemgeo.2023.121355>, 2023.](https://doi.org/10.1016/j.chemgeo.2023.121355)
- 900 [Kim, S. T., Mucci, A., and Taylor, B. E.: Phosphoric acid fractionation factors for calcite and aragonite between 25 and 75 °C: revisited, \*Chemical Geology\*, 246, 135-146, <https://doi.org/10.1016/j.chemgeo.2007.08.005>, 2007.](https://doi.org/10.1016/j.chemgeo.2007.08.005)
- King, T. M., Rosenheim, B. E., Post, A. L., Gabris, T., Burt, T., and Domack, E. W.: Large-scale intrusion of circumpolar deep water on Antarctic margin recorded by stylasterid corals, *Paleoceanography and Paleoclimatology*, 33(11), 1306–1321, <http://doi.org/10.1029/2018PA003439>, 2018.
- 905 Kurtz, D. D. and Bromwich, D. H.: A recurring, atmospherically forced polynya in Terra Nova Bay, in: *Oceanology of the Antarctic Continental Shelf*, vol. 43, edited by: Jacobs, S., American Geophysical Union, Washington, D. C., USA, 177–201, 1985.
- [Lécuyer, C., Hutzler, A., Amiot, R., Daux, V., Grosheny, D., Otero, O., Martineau, F., Fourel, F., Balter, V. and Reynard, B.: Carbon and oxygen isotope fractionations between aragonite and calcite of shells from modern molluscs, \*Chemical Geology\*, 332, pp. 92-101, <http://doi.org/10.1016/j.chemgeo.2012.08.034>, 2012.](https://doi.org/10.1016/j.chemgeo.2012.08.034)
- 910 Matsuoka, K., Skoglund, A., Roth, G., de Pomereu, J., Griffiths, H., Headland, R., Herried, B., Katsumata, K., Le Brocq, A., Licht, K., Morgan, F., Neff, P. D., Ritz, C., Scheinert, M., Tamura, T., Van de Putte, A., van den Broeke, M., von Deschwandan, A., Deschamps-Berger, C., Van Liefferinge, B., Tronstad, S., and Melvær, Y.: Quantarctica, an integrated mapping environment for Antarctica, the Southern Ocean, and sub-Antarctic islands, *Environ. Modell. Softw.*, 140, 105015, <https://doi.org/10.1016/j.envsoft.2021.105015>, 2021.
- 915 McConnaughey, T.: 13C and 18O isotopic disequilibrium in biological carbonates: I. Patterns, *Geochim. Cosmochim. Ac.*, 53, 151-162, [https://doi.org/10.1016/0016-7037\(89\)90282-2](https://doi.org/10.1016/0016-7037(89)90282-2), 1989a.
- McConnaughey, T.: 13C and 18O isotopic disequilibrium in biological carbonates II. In vitro simulation of kinetic isotope effects, *Geochim. Cosmochim. Ac.*, 53, 163–171, [https://doi.org/10.1016/0016-7037\(89\)90283-4](https://doi.org/10.1016/0016-7037(89)90283-4), 1989b.
- 920 McCrea, J. M.: On the Isotopic Chemistry of Carbonates and a Paleotemperature Scale, *J. Chem. Phys.*, 18, 849–857, <https://doi.org/10.1063/1.1747785>, 1950.
- Mikkelsen, N., Erlenkeuser, H., Killingley, J. S., and Berger, W. H.: Norwegian corals: radiocarbon and stable isotopes in *Lophelia pertusa*, *Boreas*, 11, 163–171, <https://doi.org/10.1111/j.1502-3885.1982.tb00534.x>, 2008.

- 925 Miller, K. J., Mundy, C. N., and Chadderton, W. L.: Ecological and genetic evidence of the vulnerability of shallow-water populations of the stylasterid hydrocoral *Errina novaezelandiae* in New Zealand's fiords. *Aquat. Conserv.*, 14(1), 75–94, <https://doi.org/10.1002/aqc.597>, 2004.
- [Moseley, H. N.: XIV. The Croonian lecture. —On the structure of the stylasteridæ, a family of the hydroid stony corals, Phil. Trans. R. Soc., 169, 425–503, https://doi.org/10.1098/rstl.1878.0014, 1878.](https://doi.org/10.1098/rstl.1878.0014)
- 930 Mougnot, J., B. Scheuchl, and E. Rignot. 2017. MEaSURES Antarctic Boundaries for IPY 2007–2009 from Satellite Radar, Version 2 [Coastline and grounding line], Boulder, Colorado USA. NASA National Snow and Ice Data Center Distributed Active Archive Center, <http://dx.doi.org/10.5067/AXE4121732AD>, <https://nsidc.org/data/nsidc-0709/versions/2>, 2022.
- O'Neil, J. R., Clayton, R. N., and Mayeda, T. K.: Oxygen Isotope Fractionation in Divalent Metal Carbonates, *J. Chem. Phys.*, 51, 5547–5558, <https://doi.org/10.1063/1.1671982>, 1969.
- Philipp, E., Brey, T., Pörtner, H.-O., and Abele, D.: Chronological and physiological ageing in a polar and a temperate mud clam, *Mech. Ageing Dev.*, 126, 598–609, <https://doi.org/10.1016/j.mad.2004.12.003>, 2005.
- 935 Pica, D., Cairns, S. D., Puce, S., and Newman, W. A.: Southern hemisphere deep-water stylasterid corals including a new species, *Errina labrosa* sp. n. (Cnidaria, Hydrozoa, Stylasteridae), with notes on some symbiotic scalpellids (Cirripedia, Thoracica, Scalpellidae), *ZooKeys*, (472), 1, <http://doi.org/10.3897/zookeys.472.8547>, 2015.
- Picco, P., Bergamasco, A., Demicheli, L., Manzella, G., Meloni, R., and Paschini, E.: Large-scale circulation features in the Central and Western Ross Sea (Antarctica), in: *Ross Sea Ecology*, Springer, Berlin, Heidelberg, Germany, 95–105, 2000.
- 940 Puce, S., Tazioli, S., and Bavestrello, G.: First evidence of a specific association between a stylasterid coral (Cnidaria: Hydrozoa: Stylasteridae) and a boring cyanobacterium, *Coral Reefs*, 28, 177–177, <https://doi.org/10.1007/s00338-008-0411-6>, 2009.
- 945 Puce, S., Pica, D., Mancini, L., Brun, F., Peverelli, A., and Bavestrello, G.: Three-dimensional analysis of the canal network of an Indonesian Stylaster (Cnidaria, Hydrozoa, Stylasteridae) by means of X-ray computed microtomography. *Zoomorphology* 130, 85–95, <https://doi.org/10.1007/s00435-011-0120-5>, 2011.
- Ralph, R. and Maxwell, J. G. H.: Growth of two Antarctic lamellibranchs: *Adamussium colbecki* and *Laternula elliptica*, *Mar. Biol.*, 42, 171–175, <https://doi.org/10.1007/BF00391569>, 1977.
- Risk, M. J., Heikoop, J. M., Snow, M. G., and Beukens, R.: Lifespans and growth patterns of two deep-sea corals: *Primnoa resedaeformis* and *Desmophyllum cristagalli*, *Hydrobiologia*, 471, 125–131, <https://doi.org/10.1023/A:1016557405185>, 2002.
- 950 Robinson, L. F. and van de Flierdt, T.: Southern Ocean evidence for reduced export of North Atlantic Deep Water during Heinrich event 1, *Geology*, 37, 195–198, <https://doi.org/10.1130/G25363A.1>, 2009.
- Robinson, L. F., Adkins, J., Keigwin, L. D., Southon, J., Fernandez, D. P., Wang, S.-L., and Scheirer, D. S.: Radiocarbon variability in the Western North Atlantic during the Last Deglaciation, *Science*, 310, 1469–1473, <https://doi.org/10.1126/science.1114832>, 2005.
- 955 Robinson, L. F., Adkins, J. F., Frank, N., Gagnon, A. C., Prouty, N. G., Brendan Roark, E., and de Flierdt, T. van: The geochemistry of deep-sea coral skeletons: A review of vital effects and applications for palaeoceanography, *Deep-Sea Res. Pt. II: Topical Studies in Oceanography*, 99, 184–198, <https://doi.org/10.1016/j.dsr2.2013.06.005>, 2014.

- 960 Romanek, C. S., Grossman, E. L., and Morse, J. W.: Carbon isotopic fractionation in synthetic aragonite and calcite: Effects of temperature and precipitation rate, *Geochim. Cosmochim. Ac.*, 56, 419–430, [https://doi.org/10.1016/0016-7037\(92\)90142-6](https://doi.org/10.1016/0016-7037(92)90142-6), 1992.
- Román-González, A., Scourse, J. D., Butler, P. G., Reynolds, D. J., Richardson, C. A., Peck, L. S., Brey, T., and Hall, I. R.: Analysis of ontogenetic growth trends in two marine Antarctic bivalves *Yoldia eightsi* and *Laternula elliptica*: Implications for sclerochronology, *Palaeogeogr. Palaeoecol.*, 465, 300–306, <https://doi.org/10.1016/j.palaeo.2016.05.004>, 2017.
- 965 Samperiz, A., Robinson, L. F., Stewart, J. A., Strawson, I., Leng, M. J., Rosenheim, B. E., Ciscato, E. R., Hendry, K. R., and Santodomingo, N.: Stylasterid corals: A new paleotemperature archive, *Earth Planet. Sc. Lett.*, 545, 116407, <https://doi.org/10.1016/j.epsl.2020.116407>, 2020.
- Sandrini, S., Ait-Ameur, N., Rivaro, P., Massolo, S., Touratier, F., Tositti, L., and Goyet, C.: Anthropogenic carbon distribution in the Ross Sea, Antarctica, *Antarct. Sci.*, 19, 395–407, <https://doi.org/10.1017/S0954102007000405>, 2007.
- 970 Shackleton, N.: Oxygen isotope analyses and Pleistocene temperatures re-assessed, *Nature*, 215, 15–17, <https://doi.org/10.1038/215015a0>, 1967.
- Smith, J. E., Schwarcz, H. P., Risk, M. J., McConnaughey, T. A., and Keller, N.: Paleotemperatures from deep-sea corals: overcoming ‘vital effects,’ *PALAIOS*, 15, 25–32, 2000.
- Smith, J. E., Schwarcz, H. P., and Risk, M. J.: Patterns of isotopic disequilibria in azooxanthellate coral skeletons, *Hydrobiologia*, 471, 111–115, <https://doi.org/10.1023/A:1016553304276>, 2002.
- 975 Stewart, J.A., Robinson, L.F., Day, R.D., Strawson, I., Burke, A., Rae, J.W., Spooner, P.T., Samperiz, A., Etnoyer, P.J., Williams, B., Paytan, A., Leng, M.J., Häussermann, V., Wickes, L.N., Bratt, R., and Pryer, H.: Refining trace metal temperature proxies in cold-water scleractinian and stylasterid corals, *Earth Planet. Sc. Lett.*, 545, p.116412, <http://doi.org/10.1016/j.epsl.2020.116412>, 2020.
- 980 [Stewart, J. A., Strawson, I., Kershaw, J., and Robinson, L. F.: Stylasterid corals build aragonite skeletons in undersaturated water despite low pH at the site of calcification, \*Sci Rep.\* 12, 13105, <https://doi.org/10.1038/s41598-022-16787-y>, 2022.](https://doi.org/10.1038/s41598-022-16787-y)
- Stratford, P., Stewart, B. G., and Chong, A.: In situ growth rate measurements on the red hydrocoral, *Errina novaezelandiae*, in Doubtful Sound, New Zealand fjords: Researching, managing, and conserving a unique ecosystem, *New Zeal. J. Mar. Fresh.*, 35(4), 653–661. <https://doi.org/10.1080/00288330.2001.9517032>, 2001.
- 985 Swart, P. K.: Carbon and oxygen isotope fractionation in scleractinian corals: a review, *Earth-Sci. Rev.*, 19, 51–80, [https://doi.org/10.1016/0012-8252\(83\)90076-4](https://doi.org/10.1016/0012-8252(83)90076-4), 1983.
- Thresher, R., Tilbrook, B., Fallon, S., Wilson, N., and Adkins, J.: Effects of chronic low carbonate saturation levels on the distribution, growth and skeletal chemistry of deep-sea corals and other seamount megabenthos, *Mar. Ecol. Prog. Ser.*, 442, 87–99, <https://doi.org/10.3354/meps09400>, 2011.
- 990 Urey, H. C.: The thermodynamic properties of isotopic substances, *J. Chem. Soc. (Resumed)*, 562–581, <https://doi.org/10.1039/jr9470000562>, 1947.
- Urushihara, Y., Hasegawa, H., and Iwasaki, N.: X-ray micro-CT observation of the apical skeleton of Japanese white coral *Corallium konojoi*, *J. Exp. Mar. Biol. Ecol.*, 475, 124–128, <https://doi.org/10.1016/j.jembe.2015.11.016>, 2016.



Visbeck, M.: Calibrated Hydrographic Data from the Ross Sea acquired with a CTD during the Nathaniel B. Palmer expedition NBP0402 (2004), Interdisciplinary Earth Data Alliance [CTD/Rosette], <http://doi.org/10.1594/IEDA/307431>, 2015.

995 Weber, J. N.: Deep-sea ahermatypic scleractinian corals: isotopic composition of the skeleton, *Deep-Sea Res. and Oceanographic Abstracts*, 20, 901–909, [https://doi.org/10.1016/0011-7471\(73\)90108-3](https://doi.org/10.1016/0011-7471(73)90108-3), 1973.

Weber, J. N. and Woodhead, P. M. J.: Carbon and oxygen isotope fractionation in the skeletal carbonate of reef-building corals, *Chem. Geol.*, 6, 93–117, [https://doi.org/10.1016/0009-2541\(70\)90009-4](https://doi.org/10.1016/0009-2541(70)90009-4), 1970.

1000 [Weber, J. N. and Woodhead, P. M. J.: Stable isotope ratio variations in non-scleractinian coelenterate carbonates as a function of temperature. \*Mar. Biol.\*, 15, 293–297, <https://doi.org/10.1007/BF00401388>, 1972.](https://doi.org/10.1007/BF00401388)

Wisshak, M., López Correa, M., Zibrowius, H., Jakobsen, J., and Freiwald, A.: Skeletal reorganisation affects geochemical signals, exemplified in the stylasterid hydrocoral *Errina dabneyi* (Azores Archipelago), *Mar. Ecol. Prog. Ser.*, 397, 197–208, <https://doi.org/10.3354/meps08165>, 2009.

1005 Wisshak, M., Form, A., Jakobsen, J., and Freiwald, A.: Temperate carbonate cycling and water mass properties from intertidal to bathyal depths (Azores), *Biogeosciences*, 7, 2379–2396, <https://doi.org/10.5194/bg-7-2379-2010>, 2010.

WOCE Hydrographic Programme, WHP: Hydrochemistry measured on water bottle samples during Akademik Ioffe cruise 90KDIOFFE6\_1 on section S04P, PANGAEA [CTD/Rosette], <https://doi.org/10.1594/PANGAEA.837058>, 2002.